ACS OMEGA

Open Access

http://pubs.acs.org/journal/acsodf

Article

Petrophysical Evaluation of a Shaly Sandstone Reservoir and the Effect of Clay Minerals on Reservoir Quality: A Case Study from the Barremian Mengo Sandstone, Kouilou Basin, Republic of Congo

Armel Prosley Mabiala Mbouaki,* Zhongxian Cai, Elia Wilinasi Sikanyika, Grant Charles Mwakipunda, and Hugues Roland Konan

Cite This: *ACS Omega* 2025, 10, 10081−10106

Read Online

ACCESS | Metrics & More | Article Recommendations

ABSTRACT: The growing global demand for energy is driving specialists to reevaluate and exploit fossil fuel deposits previously considered economically unviable. This study addresses the challenge of evaluating the Mengo shaly sandstone reservoir, a fan sandstone that is affected by diagenesis and that has heterogeneous porosity and low permeability and was abandoned due to its poor petrophysical properties, in the Kouilou Basin, Republic of Congo, particularly the impact of clay minerals on reservoir quality. The significance of this study lies in addressing the complex challenges associated with evaluating and exploiting shaly sandstone reservoirs, which are increasingly important for meeting global energy demands. The study involved integrating well logs, core data, and well testing data from 14 wells, with a focus on seven, using techniques such as the Schlumberger Techlog software; gamma ray, density, neutron, sonic, and resistivity logs; core analysis to measure porosity, permeability, and lithology; Xray diffraction; and scanning electron microscopy for mineral identification. The results indicated a reservoir composition of poorly sorted coarse and fine-grained lithologies with a significant clay content. Chlorite was identified as the primary clay mineral affecting porosity and permeability, with porosity values ranging from 8 to 15% and permeability values averaging from 0.16 to 1.68 mD. The study identifies diagenetic processes, such as the presence of clay minerals, as the primary cause of the contrast between porosity and permeability by reducing reservoir quality. Despite the challenges posed by the high clay content and radioactivity, integrating log and core data into a conceptual geological model is crucial for accurate reservoir characterization. The Midfan area around the MEN-105 well is pinpointed as the most favorable zone for future drilling.

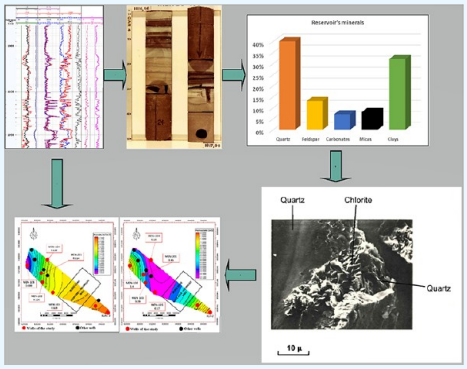

1. INTRODUCTION

The escalating global demand for energy is compelling experts to reassess and develop fossil fuels, especially oil and gas reserves that were once deemed economically unviable. As global energy demand is projected to grow significantly by 16% to 54% in the coming decades, there is increasing pressure on energy systems to meet this demand, particularly in emerging economies where energy needs are rapidly expanding.[1] This reassessment is crucial to satisfy the energy needs of an increasingly industrialized world. One potential solution to this high demand lies in evaluating and exploiting shaly sandstone reservoirs characterized by high clay content and suboptimal petrophysical properties. Clay minerals in shaly sandstone reservoirs play a pivotal role in determining reservoir quality by significantly influencing porosity, permeability, and fluid saturation.[2] The distribution, type, and quantity of these minerals within the reservoir matrix can alter rock properties and complicate the interpretation of well-logging, core, and well-testing data.[3,4]

Accurate characterization of clay content in shaly sandstone reservoirs is crucial for understanding mineral composition and its effects on reservoir quality.[5] To this end, several analytical methods are commonly employed. These include X-ray diffraction (XRD) for clay mineral identification, scanning electron microscopy (SEM) for imaging clay structure and distribution, gamma-ray logging to infer clay content via natural radioactivity, and cation exchange capacity (CEC) testing to assess the reservoir's capacity for cation absorption, which correlates with clay type and quantity. Advanced techniques like spectral gamma-ray logging further refine clay content estimates by differentiating between radioactive

Received: September 16, 2024
Revised: February 2, 2025
Accepted: February 7, 2025
Published: March 6, 2025

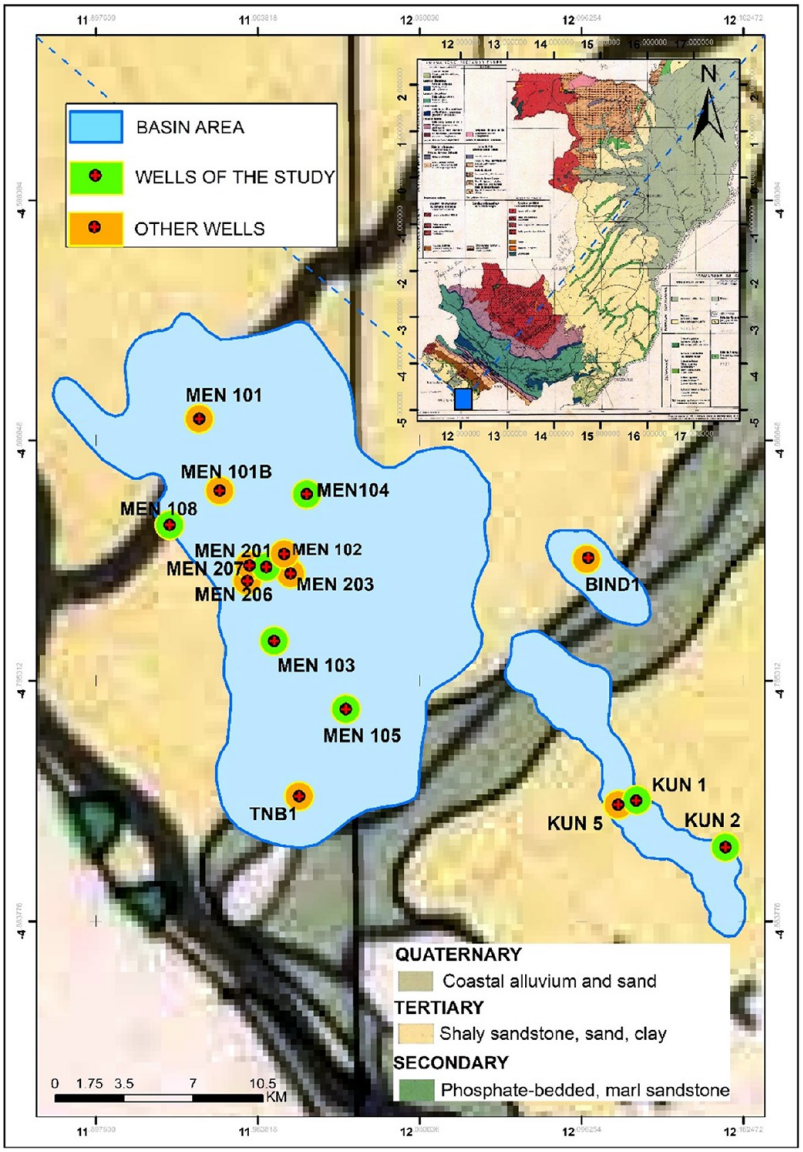

Figure 1. Location map showing Mengo, Kundji, and Bindi oilfields targeting the Mengo sandstone reservoir in the study area (Map courtesy of Armel Prosley Mabiala Mbouaki. Copyright 2024).

isotopes such as potassium, thorium, and uranium. These methods are instrumental in identifying how clay mineralogy affects pore structure and fluid dynamics. Recent studies emphasize the critical role of clay minerals in influencing the quality of sandstone reservoirs through various effects on pore structure, fluid flow, and elasticity. Al-Kharra'a et al. (2023) demonstrated that different clay types, particularly fibrous Illite and Illite platelets, impact permeability by either blocking or preserving micropore throats. other studies have examined the diagenetic origins and effects of authigenic clay minerals in tight conglomerate reservoirs. For instance, Yu, Wang, and Adenutsi (2023) showed that pore-lining chlorite coatings in the Junggar Basin enhance pore size distribution, while pore-filling chlorite aggregates decrease reservoir quality. Sayers (2023) found that nonload-bearing clay simplifies modeling of elastic properties, and Dong et al. (2024) extended these insights by examining chlorite coatings' role in porosity preservation but noted that double-layer coatings can obstruct pore throats. Additionally, Magoba, Opuwari, and Liu (2024) identified that diagenetic processes, particularly clay mineralization like glauconite, Illite, and smectite cementation, reduce connectivity in the Bredasdorp Basin, reinforcing the influence of clay minerals across various geological contexts. Together, these studies underscore the nuanced effects of clay mineral type, content, and distribution on reservoir quality and hydrocarbon recovery.

However, the challenges posed by high clay content on reservoir quality are particularly evident in economically marginal reservoirs. A prime example is the Mengo sandstone reservoir, part of the Mengo-Kundji-Bindi (MKB) oilfields in the coastal basin of the Republic of Congo. This reservoir, characterized as a fan sandstone, has been significantly affected by diagenesis, resulting in heterogeneous porosity and critically low permeability. These poor petrophysical properties ultimately led to the abandonment of the Mengo reservoir, despite its previous cumulative production of approximately 1.5 million barrels of 32°API waxy oil. The reservoir became economically unviable due to the severe reduction in permeability, highlighting the critical importance of detailed clay mineralogy analysis in reservoir characterization. The

https://doi.org/10.1021/acsomega.4c08491
ACS Omega 2025, 10, 10081−10106

Mengo sandstone serves as a cautionary tale, illustrating the impact that clay minerals, particularly their type and distribution, can have on reservoir quality. The reservoir's abandonment underscores the necessity for more sophisticated evaluation methods that can accurately characterize the spatial variability of clay mineralogy and its influence on reservoir properties.

Effective well log evaluation is essential for assessing clay mineral content and distribution in shaly sandstone reservoirs. Techniques such as gamma-ray logging, spectral gamma-ray logging, and resistivity logging provide valuable insights into clay volumes and types.[7] Gamma-ray logging is a foundational method, using natural radioactivity to estimate clay volume indirectly.[8] Spectral gamma-ray logging further differentiates clay types by analyzing contributions from potassium, thorium, and uranium. When integrated with core and well-testing data, resistivity logs help differentiate between clay-bound and free water, enhancing the accuracy of hydrocarbon estimates and reducing the risk of reserve miscalculations[1012]. Together, these methods offer a robust approach to capturing the complex relationships between clay mineralogy, porosity, and permeability, thereby improving the precision of reservoir characterizations.

Addressing these challenges, this research aims to accomplish three objectives: first, to characterize the Mengo sandstone reservoir with a focus on clay mineralogy and spatial variability; second, to quantify the impact of clay minerals on porosity and permeability; and third, to develop an integrated interpretation framework combining X-ray data, well-logging data, well-testing data, and core data. This comprehensive approach seeks to enhance reservoir characterization and inform effective hydrocarbon recovery strategies, contributing to more resilient energy solutions for an increasingly industrialized world.

2. GEOLOGICAL SETTING

2.1. Structural Setting. The Mengo sandstone lies within the inner part of the South Atlantic Margin (Figure 1), within a complex system of syn-rift horst and graben structures that form part of the Inner Atlantic Hinge Zone in the Congo Basin. The Congo Basin is one of several rift basins that formed on the South Atlantic margins as South America and Africa began to separate in the late Jurassic and early Cretaceous.[10] Furthermore, the Congo Basin is separated from the Atlantic basin of Gabon to the north and the Kwanza basin of Angola to the south by the Mayumba spur and Ambriz arch.

The Mengo sandstone is part of a series of rift basins extending NW-SE on the West African Atlantic Margin. These basins result from the breakup of South America and Africa during the opening of the Atlantic Ocean at Neocomian time. According to the petrographic and diagenetic analyses of the Mengo sandstones, the reservoir quality is predominantly controlled by the cementation and compaction processes.[11] Moreover, the structural history of the Congo Basin is closely related to the NW-SE opening trend of the Atlantic Ocean. Initially, this opening trend led to the development of intracontinental basins during the Neocomian period. Subsequently, during the Tertiary period, the basin experienced uplift due to the Afar plume in East Africa, resulting in intense erosion and high sedimentation input through deltas. The deposition of turbiditic systems followed this. Furthermore, the later stages of the rift system are characterized by thermal subsidence, transforming the environment into a lacustrine setting with the deposition of evaporite sequences.

2.2. Stratigraphic Setting. The stratigraphy along the Congolese shoreline basin belongs to the Cretaceous era (Figure 2). It is divided into two units by the Aptian Loeme

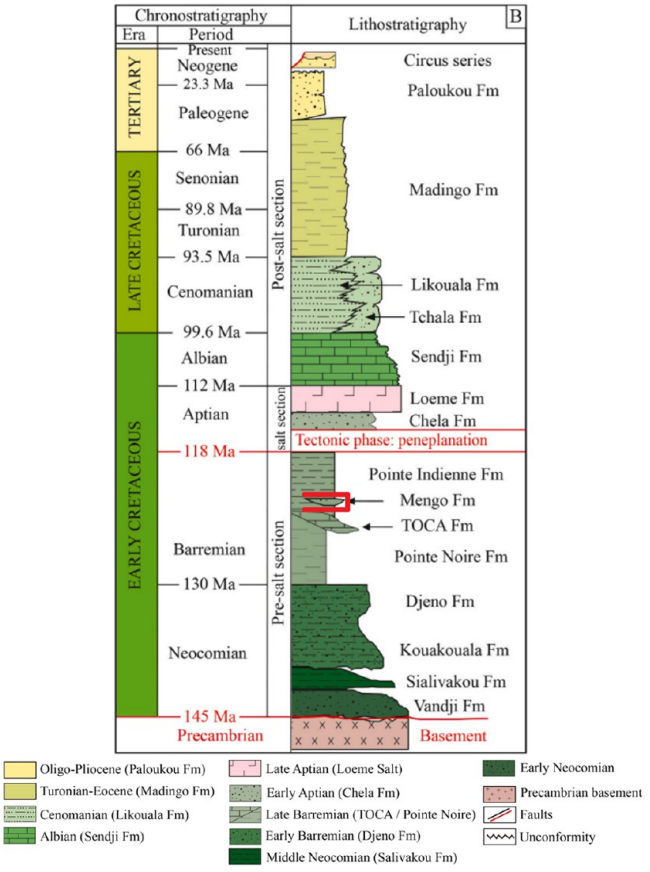

Figure 2. A generalized stratigraphic column depicting the Kouilou Basin, which is part of the Congo Basin in the Republic of the Congo, equatorial West Africa, includes information on the ages, lithology, formation names, and tectonic stages. Reprinted with permission from.[12] Copyright 2023, Elsevier.

Salt Formation: the Post-Salt and the Turonian-Albian units. The Mengo Sandstone, of the Barremian age, is situated in the lower part of the Pointe Indienne Formation, just above the top of Pointe Noire Marls. In the Mengo area, there is a vertical separation of over 100 m between the top of Pointe Noire Marls and the base of the Mengo Sandstone.

2.3. Mengo Environment Deposition. The Presalt series were deposited in a lacustrine environment. The Pointe Noire Formation, as supported by Cole et al.(2000),[13] was formed in a deep, anoxic freshwater to shallow, low-energy lacustrine environment.[13] This is evident from the presence of a high proportion of type I kerogen, indicative of lacustrine algal origin, as noted by.[10] The Pointe Indienne Formation is also recognized as a lacustrine deltaic deposit, characterized by a shift from type I kerogen to type III kerogen. This change suggests a transformation in the organic matter and nutrients supplied to the rift lake, as stated by Harris et al. (2005).[10] Upon analyzing core descriptions, no traces of paleosols or roots, which are typical of subaquatic deposition, are observed in the clays.

https://doi.org/10.1021/acsomega.4c08491
ACS Omega 2025, 10, 10081−10106

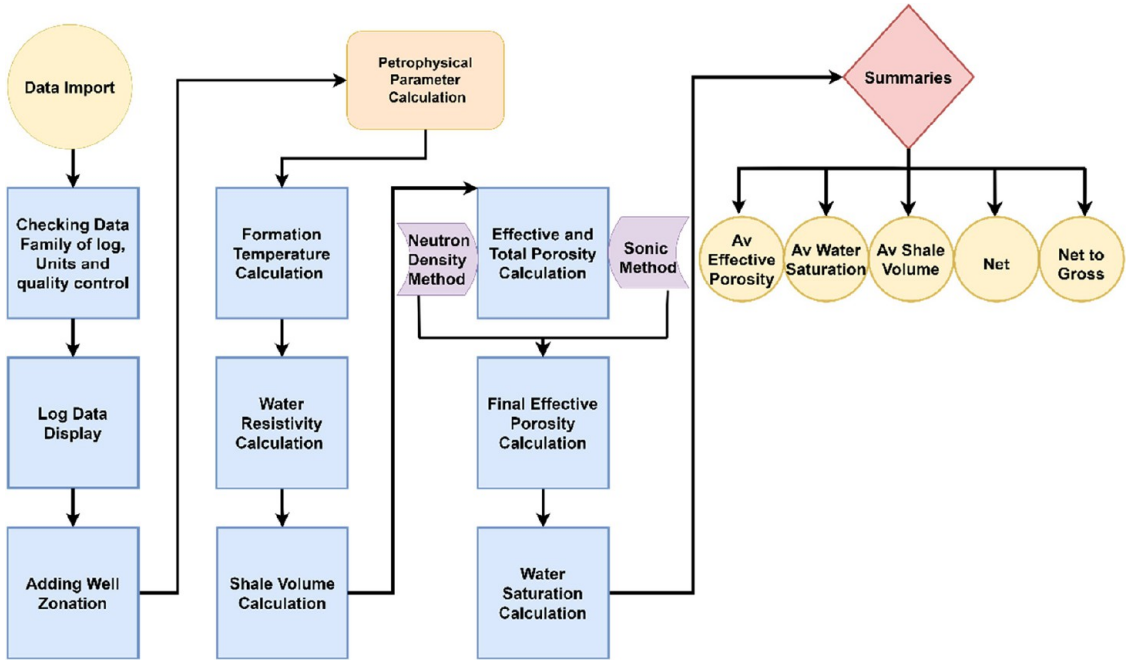

Figure 3. Workflow of the petrophysical evaluation of the studied wells.

3. METHODOLOGY

3.1. Data Collection. The study utilized field data from the Mengo Kundji Bindi (MKB) oilfield in the Kouilou Basin, Republic of Congo, collected from 14 wells. Among these, seven wells (MEN-103, MEN-104, MEN-105, MEN-108, MEN-201, KUN-1, and KUN-2) were initially selected, but only five (MEN-103, MEN-104, MEN-105, MEN-108, and MEN-201) were used due to the lack of major logs in two wells. These five wells were evaluated using conventional well logging techniques and core data, including routine core analysis for porosity and permeability, lithological data, mineralogical analysis, and well-testing data. The suite of well logging tools included gamma ray (GR), caliper (CAL), density (DEN), density correction (DRHO), neutron (NPHI), compressional slowness (DT), shallow Laterolog resistivity (LLS), deep Laterolog resistivity (LLD), and deep induction log resistivity (ILD). These logs were used to assess petrophysical properties and the influence of clay minerals on the quality of the Mengo sandstone reservoir. Core plugs collected from various intervals of the Mengo sandstone formation were analyzed for mineralogical composition, core porosity, and core permeability. Additionally, unpublished reports from the Congolese National Petroleum Company (SNPC) were utilized in the study.

3.2. Well Logging and Core Analysis. Evaluating a sandstone reservoir using well-logging and core data is a complex process that requires a detailed understanding of the formation's petrophysical properties. This paper outlines a methodology for assessing sandstone reservoirs to optimize hydrocarbon production. The first step is collecting well-logging data, including key logs such as the Gamma Ray log, which measures natural γ radiation to identify lithology and shale content; the Density log, which measures formation density to determine porosity and lithology; the Neutron log, which assesses the neutron capture cross-section to determine porosity; the Sonic log, which measures sound speed in the formation to evaluate porosity and lithology; and the Resistivity log, which measures electrical resistivity to determine porosity and water saturation. This comprehensive approach enables a thorough evaluation of the shaly sandstone reservoir's petrophysical properties.

3.2.2. Data Processing and Quality Control. After the company experts processed the data to remove noise and artifacts, the next step was quality control to ensure the logs were accurate and error-free. The validated logs were then interpreted to determine the formation's petrophysical properties. Gamma ray logs identified lithology, with high and low readings indicating shale and sandstone. The neutron-density crossplot was used to identify lithology within the sandstone, limestone, and dolomite pattern diagram. Density, neutron, and sonic logs measured porosity, and a combination of these logs provided a precise porosity estimation. This comprehensive approach accurately interpreted the shaly sandstone reservoir's petrophysical properties.

3.2.4. Core Samples. Core samples are extracted from the formation and analyzed in the laboratory to obtain accurate measurements of porosity, permeability, and lithology. The core analysis process involves several steps: extracting cores using a coring tool, preparing the samples by cleaning them, and then conducting the analysis. The well log and core data are integrated to understand the reservoir properties through a series of steps comprehensively. First, depth matching is performed to align the depth of the core samples with the well logs. Next, the calibration process involves adjusting the well-log data using the core data. Finally, correlation aligns the well-log data with the core data to obtain more accurate estimates of the petrophysical properties. This integration ensures a detailed and precise understanding of the reservoir.

3.2.6. Reservoir Characterization. The integrated well log and core data are used to characterize the reservoir, including determining the reservoir thickness and the distributions of porosity, permeability, lithology, and fluid saturation. Figure 3 below illustrates the workflow for the petrophysical evaluation of the Mengo Shaly sandstone reservoir.

https://doi.org/10.1021/acsomega.4c08491
ACS Omega 2025, 10, 10081−10106

3.3. Petrophysical Evaluation. *3.3.1. Data Loading.* The raw data were loaded into Schlumberger Techlog software in LAS format, covering a much larger interval. However, the interpretation was filtered and narrowed down specifically to the Mengo reservoir, especially the Top Mengo, the area of interest.

3.3.2. Formation Temperature. The method used in this study to calculate formation temperature is the TLI/BLI interval equation, as shown in eq 1:

$$FTEMP = TFT + \frac{(BLT - TLT) \times (depth - TLI)}{(BLI - TLI)} \quad (1)$$

Where *TLI* is Top log interval in meter, *TLT* is Top log temperature in degrees Celsius *BLI* is Bottom log interval in meter, *BLT* is Bottom log temperature in degrees Celsius

3.3.3. Water Resistivity from Temperature and Spontaneous Potential. The method utilizes formation water resistivity and salinity, along with temperature and spontaneous potential at 75 °F to calculate mud filtrate resistivity using the equations (eqs 2 to 10):

$$R_{MF75} = R_{MF} x \frac{T_{MF} + 7}{75 + 7} \quad (2)$$

$$R_{MF75} = \begin{cases} \text{if} R_{MF75} < 0.10 \\ else: \end{cases} \quad (3)$$

$$\frac{146 R_{MF75} - 5.0}{337 x R_{MF75} + 77} = > 0.35 \times R_{MF75} \quad (4)$$

$$R = 10^{-SP/60.0 + 0.133 \times T} \quad (5)$$

$$R_{w_{Eq75}} = \frac{R_{MFEq75}}{R} \quad (6)$$

$$R_{W75} = \begin{cases} \text{if} R_{WEq75} < 0.10 \\ else: \end{cases} \quad (7)$$

$$0.03793 + 0.22248 \text{XR}_{\text{WEq75}} + 14.87084^2 \text{XR}_{\text{WEq75}} - 80.77638^3 \text{xR}_{\text{WEq75}} \quad (8)$$

$$0.02093 + 1.12581 \text{xR}_{\text{WEq75}} - 0.62131^2 \text{xR}_{\text{WEq75}} + 1.68355^3 \text{xR}_{\text{WEq75}} \quad (9)$$

Formation water resistivity

$$R_W = R_{W75} X \frac{82.0}{T + 7.0} \quad (10)$$

According to Mutti. E (1992),[14] petrophysics involves studying the physical and chemical characteristics of rocks and the fluids they contain; it offers essential data for understanding subsurface formations and assessing the potential of resources.[15] During drilling operations, various properties are determined, including lithology, shale volume, shale porosity, fluid type, water saturation, formation permeability, formation pressure, and formation mobility. Accurate and corrected data are essential for calculating these properties. LWD of Mengo measurements perform borehole environmental adjustments on the raw data, eliminating the influence of mud and borehole size to ensure precise measurements. Various petrophysical models are employed to analyze complex and heterogeneous reservoirs to provide reliable results that align with production statistics and core sample research findings.

3.3.4. VShale from Gamma Ray. The final shale volume (VSH) was determined by selecting the method that produced the lowest estimated shale volume, known as the minimal shale volume. This process involved using both Gamma Ray and neutron/density/sonic shale volume calculations. The minimum VSH value is typically chosen because most VSH calculation algorithms tend to overestimate shale volume.[16] The Gamma-ray shale volume method uses a general linear equation, as shown in eqs 11 and 12, to calculate the shale volume with the GR curve as the sole input.

$$GR_{index} = \frac{GR - GR_{matrix}}{GR_{shale} - GR_{matrix}} \quad (11)$$

$$\text{VSH} = GR_{index} = \frac{GR - GR_{matrix}}{GR_{shale} - GR_{matrix}} \quad (12)$$

3.3.5. Porosity by Neutron Density Method. After exploring various combinations of conventional computation methods, the effective porosity and total porosity were computed using the neutron density method.[8] These calculations involved utilizing a density/neutron cross plot and a porosity with sonic/neutron cross plot. The method for calculating the final total porosity (PHIT) depends on the data quality and the influence of the borehole. By applying the standard equation (*PHIE = PHIT (1 - VSH)s*, eq 13, the effective porosity (PHIE) was determined by incorporating the shale volume correction into the final total porosity calculation. Consequently, the effective porosity was derived.

$$\phi_d = \frac{\rho_b - \rho_{\text{lim}}}{\rho_{mf} - \rho_{\text{lim}}} \quad (13)$$

Where ρ_b is Bulk density ρ_{lim} is Limestone grain density, default 2.71 g/cm^3 ρ_{mf} is Mud filtrate density, default 1 g/cm^3 or bulk density fluid parameter, ρ_{sand} is Sandstone grain density default 2.65 g/cm^3, ρ_{dol} is Dolomite grain density, default 2.9 g/cm^3, ϕ_n is Neutron porosity, ϕ_d is Density porosity

3.3.6. Water Saturation. The Indonesia equation technique, proposed by Moon et al.(1998),[16] was used to calculate water saturation (Sw) due to inaccuracies in resistivity data, with residual oil saturation (ROS) determined through swept zone logging. Initially, the Archie and Indonesian equations were applied to determine water saturation. However, the Archie method indicated almost complete water saturation in the reservoir, while the Indonesian method provided more reliable results, considering additional reservoir information. Core studies further demonstrated that the Indonesian method closely matched the actual fluid saturation in the Mengo reservoir, especially in the five wells studied. Therefore, we concluded that the Indonesian equation is better suited for water saturation calculations in this reservoir. The Archie method proved inaccurate for the Mengo sandstone reservoir, which has significant clay content and is not a clean formation suitable for the Archie method.[17] Consequently, formation water saturation was determined using the Indonesian eq (eqs 14 to18).[8]

$$R_0 = \frac{a \times R_w}{\text{Ø}^m} \quad (14)$$

$$c = 1 - (v_{sh} x 0.5) \quad (15)$$

https://doi.org/10.1021/acsomega.4c08491
ACS Omega 2025, 10, 10081−10106

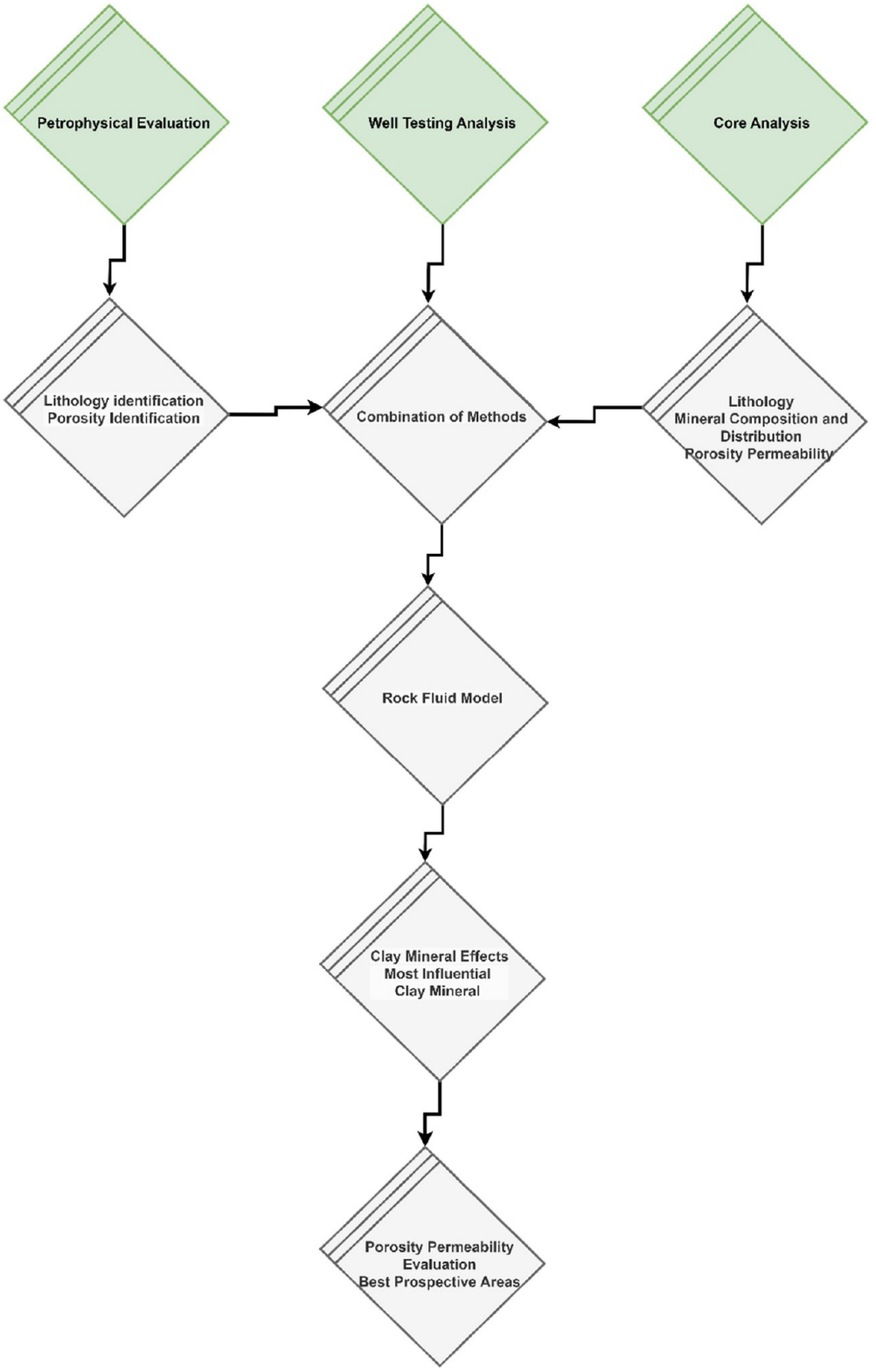

Figure 4. General workflow of the study.

$$A = \frac{V_{sh}^{C}}{\left(\frac{R_{sh}}{Rt}\right)^{0.5}} \quad (16)$$

$$B = \left(\frac{R_t}{R_0}\right)^{0.5} \quad (17)$$

$$S_w = (A + B)^{-2/n} \quad (18)$$

Where a is the Tortuosity exponent; m is the Cementation exponent n is the Saturation exponent R_w is Water resistivity R_{sh} is the Resistivity log reading in 100 shale; Rt is Formation resistivity and S_w is Formation water saturation

https://doi.org/10.1021/acsomega.4c08491
ACS Omega 2025, 10, 10081−10106

3.3.7. Net Reservoir and Net Pay Determination. Log cutoffs are a conventional approach used to identify net reservoir rocks that contribute to reservoir production or provide pressure support, with permeability being the principal parameter governing these contributions. The log-based permeability estimate (K) is determined by effective porosity (PHIE) and shale volume (Vsh). To establish net reservoir zones, cutoffs for Vsh and PHIE are first applied, followed by a water saturation (Sw) cutoff to identify net pay, defining the producible water and hydrocarbon quantities. While identifying high-quality reservoirs is straightforward, locating marginal reservoirs with higher shale concentrations and lower effective porosity is more challenging. This requires meticulous data examination and comparison to analogous productive reservoirs in other wells. Therefore, the final petrophysical evaluation employs distinct cutoffs for Vsh, PHIE, and Sw to account for these variations.

3.3.8. Permeability Calculation. The permeability of a reservoir is significantly influenced by factors such as heterogeneity, lithology, texture, pore connectivity, and pore throat size distributions. The presence of shale adversely affects permeability. Permeability values are commonly derived from the relationship between core permeability and either core porosity or log porosity. In core studies, six porosity-to-permeability algorithms are developed based on specific ranges of shale volume (Vsh) and effective porosity (ϕ). These algorithms help to identify different K-transforms (eq 19), improving the understanding of the reservoir's permeability heterogeneity and providing reliable permeability data for defining flow units or "flow facies". This method enhances the accuracy of permeability data.[16] The key steps of this work's entire process are summarized in Figure 4.

$$k = \frac{10^{(\phi - c)/b}}{\phi} \tag{19}$$

Where: k is Permeability (mD); ϕ is Effective porosity (v/v); c and b are Constants based on the K-transform group, effective porosity and shale volume

4. RESULTS

The primary objective of the petrophysical analysis using well logs is to determine the thickness of the pay zone and estimate the hydrocarbon volume within the formation. This analysis was conducted using Schlumberger TechLog software. Well logs from five wells (MEN-103, MEN-104, MEN-105, MEN-108, and MEN-201) were analyzed to determine lithology, mineral composition, net pay, effective porosity, clay volume, and fluid saturations.

4.1. Well-Logging. The Rw value, based on the reservoir water salinity of 150 K ppm obtained from well tests in wells MEN-103 and MEN-108, was calculated using the resistivity of the NaCl solution. The calculated Rw values are as follows: 0.02214 Ohmm at 89 °C for wells MEN-103, MEN-104, and MEN-105; 0.0241 Ohmm at 80 °C for well MEN-108; and 0.02234 Ohmm at 88 °C for well MEN-201. These values were determined using an abacus for precise calculation.

The estimation of clay volume in the Mengo sandstone reservoir relied on four logs: Gamma Ray (GR), Neutron, Density, and Resistivity, with the minimum value among these logs selected as the final clay volume (Vclay). Chlorite and Illite were identified as the most significant clay minerals. The RHOB/NPHI tool was calibrated for a limestone matrix, necessitating a correction for the hydrogen index porosity to account for the sandstone reservoir. A corrected NPHI curve was computed using lithology-porosity charts for the CNL Neutron Index, adding four porosity units (PU) to the existing NPHI curve. Porosity was calculated using the Neutron-density model. The Indonesia equation was applied for water saturation computation, as it is known to yield reliable results in shaly sandstone formations in Congo. Figure 5 below illustrates the different logs used for these computations.

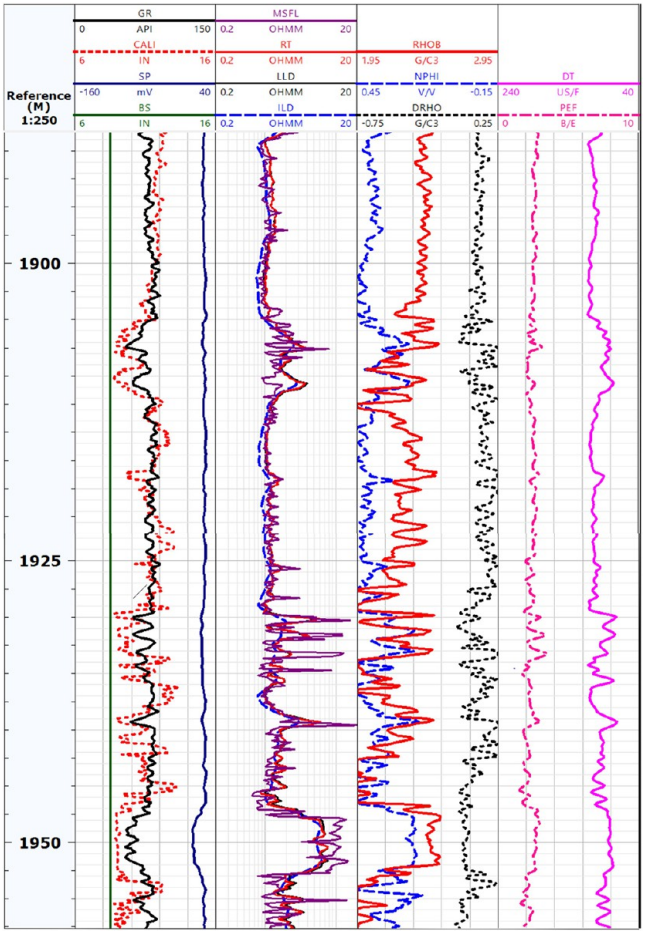

Figure 5. Visualization of different welll logs used in this study.

The quality control of the petrophysical model was performed by comparing it with conventional core descriptions, revealing a strong correlation between the model's lithology and core analysis lithology, thereby confirming the model's robustness and accuracy. Four parameters were used to define cutoff criteria for summation calculations and determine the net reservoir and net pay. Permeability cutoff, derived from core laboratory data, indicated that reservoir flow begins at 0.1 mD, a threshold deemed acceptable due to natural enhancements from trapped methane and preproduction fracturing. For porosity cutoff determination, the calibration of core-log data was essential to identify which log porosity total porosity (PHIT) or effective porosity (PHIE) correlated with core porosity. The results demonstrated that core porosity aligned more closely with total porosity (PHIT), underscoring its reliability for reservoir evaluation and summation calculations.

https://doi.org/10.1021/acsomega.4c08491
ACS Omega 2025, 10, 10081−10106

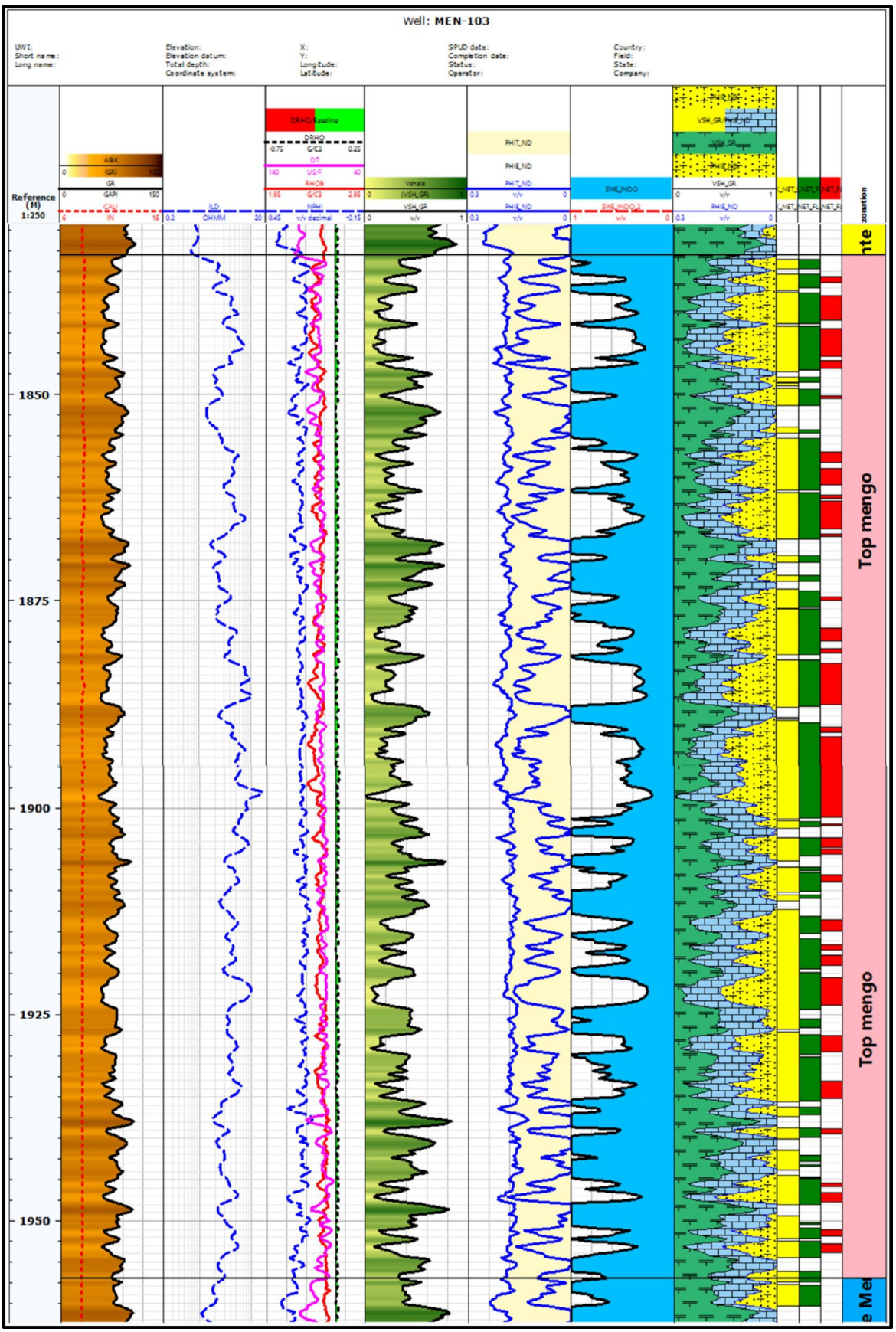

Figure 6. Interpretation composite log of well MEN-103.

https://doi.org/10.1021/acsomega.4c08491
ACS Omega 2025, 10, 10081−10106

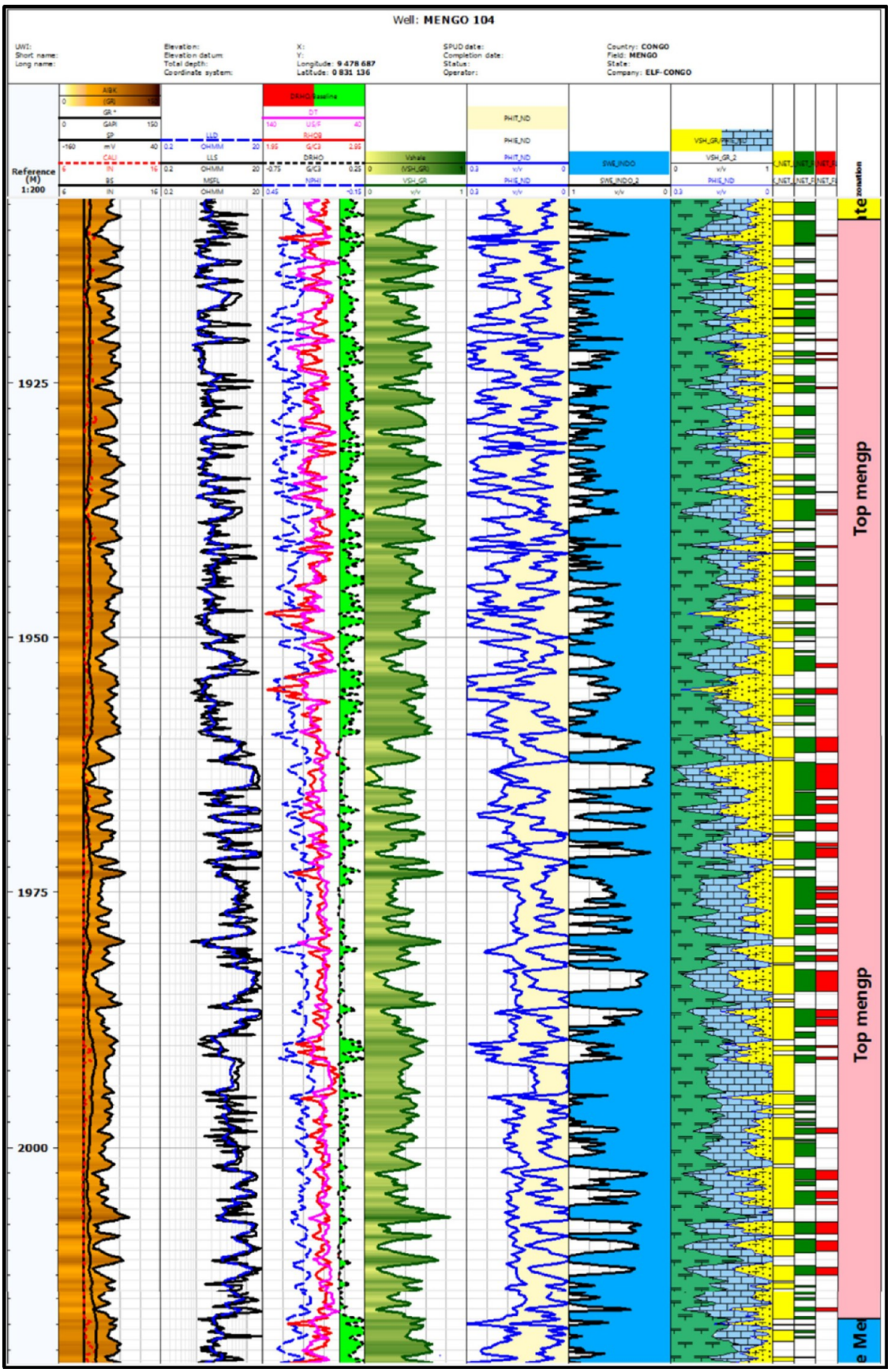

Figure 7. Interpretation composite log of well MEN-104.

https://doi.org/10.1021/acsomega.4c08491
ACS Omega 2025, 10, 10081−10106

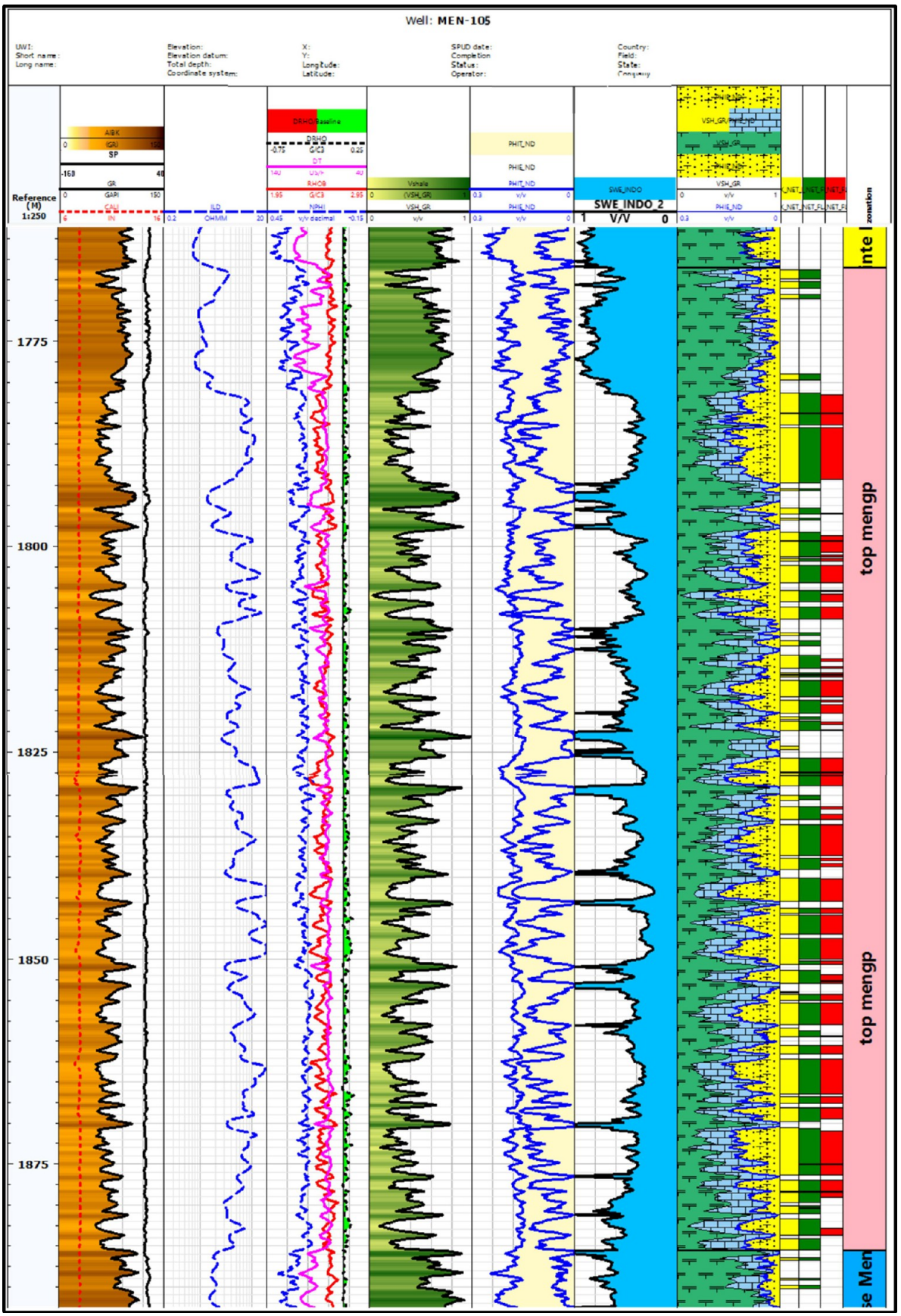

Figure 8. Interpretation composite log of well MEN-105.

https://doi.org/10.1021/acsomega.4c08491
ACS Omega 2025, 10, 10081−10106

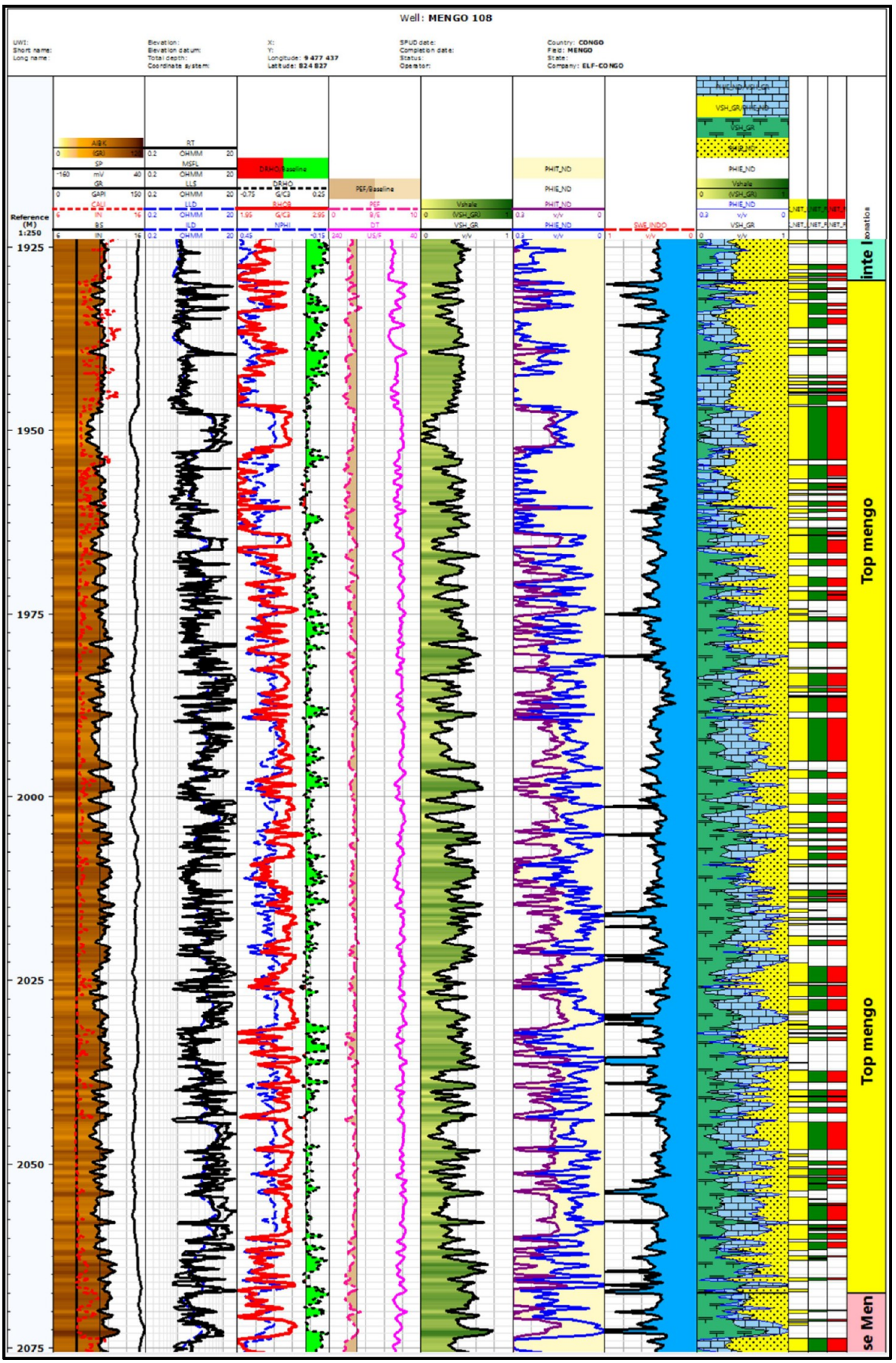

Figure 9. Interpretation composite log of well MEN-108.

https://doi.org/10.1021/acsomega.4c08491
ACS Omega 2025, 10, 10081−10106

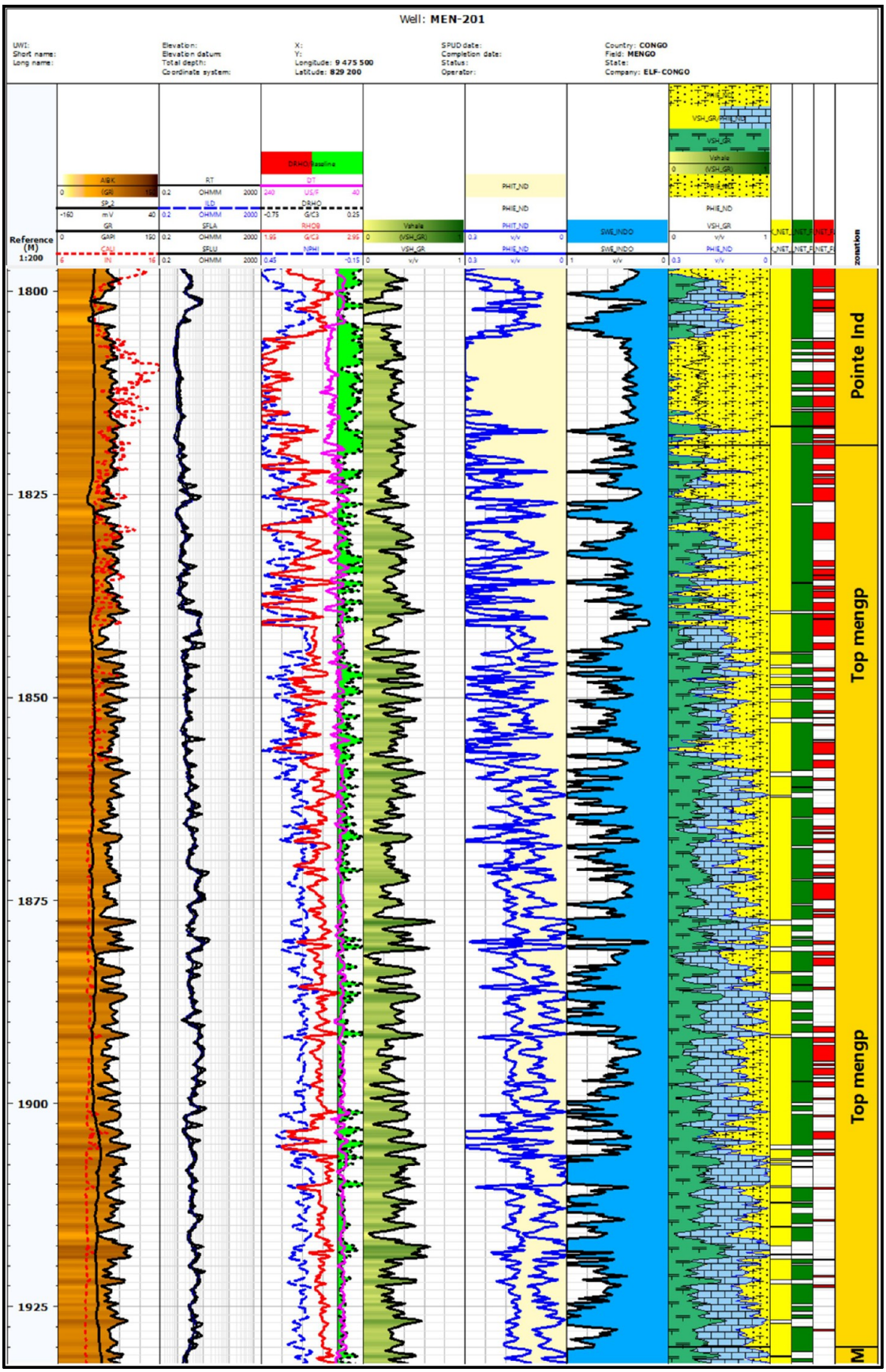

Figure 10. Interpretation composite log of well MEN-201.

https://doi.org/10.1021/acsomega.4c08491
ACS Omega 2025, 10, 10081−10106

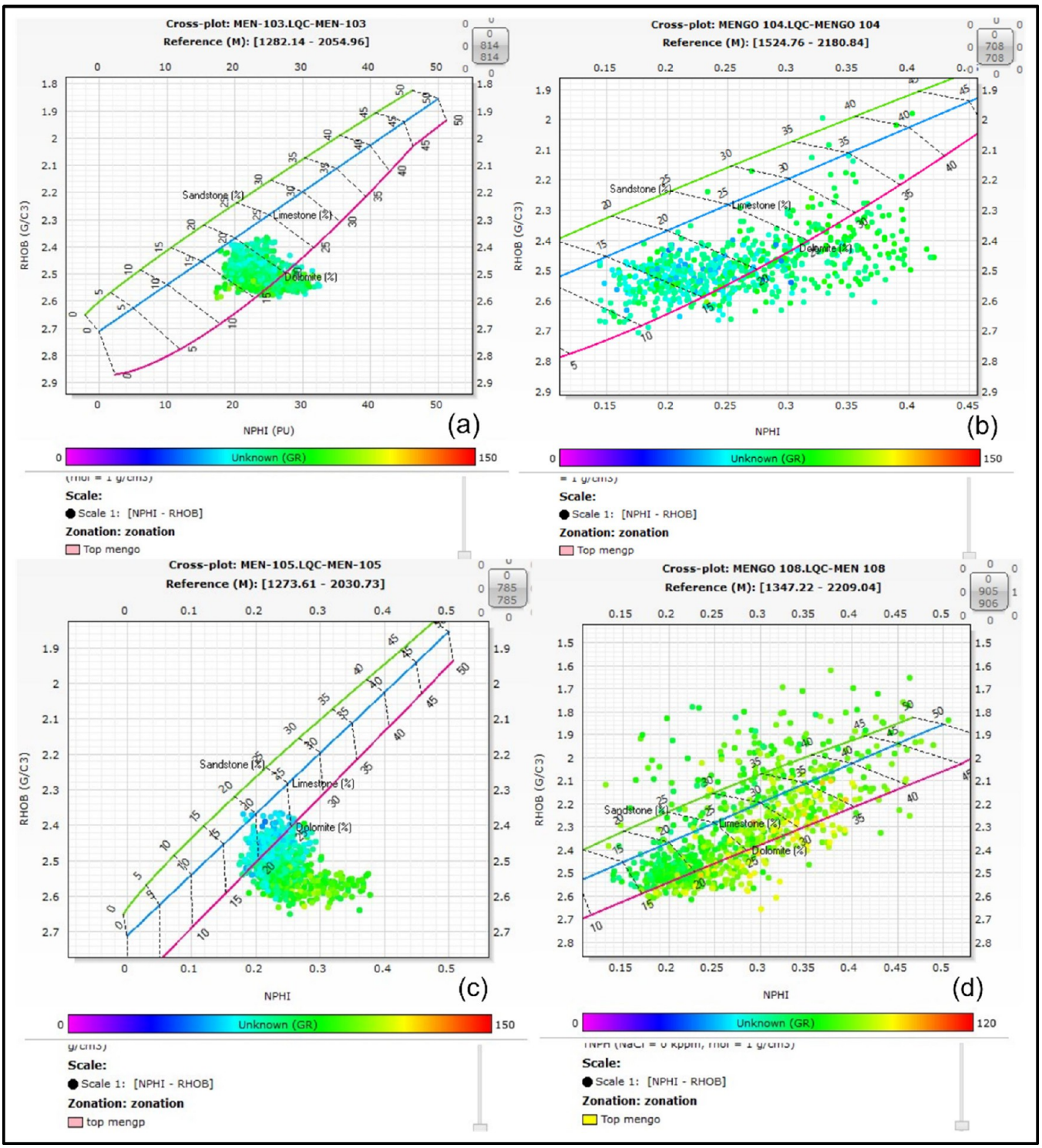

Figure 11. Lithological cross plot of the studied wells. (a) shows a cross-plot representation with no plots along the sand and limestone lines, proving unclean sandstone lithology. (b) exhibits a widespread of plots. (c) represents a plot showing a possible shaly lithology. (d) displays the most extensive spread of plots.

The petrophysical evaluation of the Mengo shaly sandstone reservoir was conducted using Schlumberger's Techlog software, providing a comprehensive analysis of reservoir properties. The results are illustrated through five figures (from Figures 6 to 10), each displaying key petrophysical logs used to interpret the reservoir parameters. These parameters include the shale volume in green, total and effective porosity in gray, water saturation in blue, and the pay zones in red, located adjacent to the zonation track. The "Top Mengo" marker within the zonation track denotes the reservoir zone of interest, which is divided into several subzones labeled A through F. This evaluation offers detailed insights into the reservoir's heterogeneity, helping to identify productive zones and assess their potential for hydrocarbon exploitation.

The well MEN-105 is situated in the southernmost region of the field. The use of oil-based mud (OBM) during drilling

https://doi.org/10.1021/acsomega.4c08491
ACS Omega 2025, 10, 10081−10106

Table 1. Summary of Reservoir Results of the Five Wells of the Study

	rock					reservoir			pay				
	top	bot	gross	net	N/G	poro	Sw	VSh	net	N/G	Poro	Sw	VSh
model	MD					average			MD			average	
MEN **103**	1833	1957	113	99.7	0.804	0.094	0.538	0.298	50.597	0.447	0.116	0.42	0.205
MEN **104**	1909	2017	96.5	77.1	0.714	0.067	0.635	0.338	22.86	0.236	0.118	0.41	0.235
MEN **105**	1766	1885.5	109.5	56.54	0.473	0.118	0.45	0.268	77.61	0.705	0.128	0.39	0.266
MEN **108**	1929.5	2067.5	118	72.43	0.525	0.112	0.428	0.253	65.11	0.551	0.088	0.40	0.255
MEN **201**	1819	1930	111	89.36	0.805	0.122	0.536	0.287	37.38	0.337	0.114	0.40	0.283

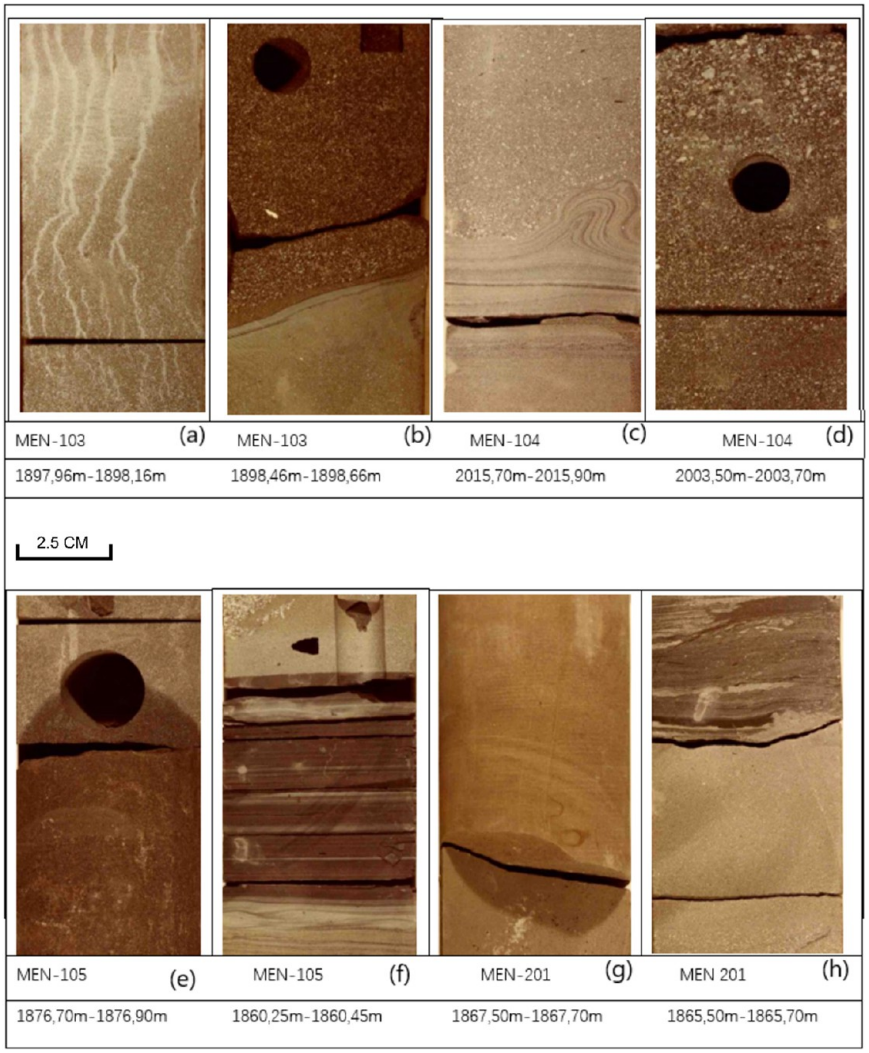

Figure 12. Core samples from the Mengo Sandstone Reservoir across different wells: (a) Fluidized sandstone with vertical pipes and calcite cement, and (b) sand-silt discontinuity from Well Men 103; (c) flame structures, and (c) coarse-grained sandstone lithology from Well Men 104; (e) fine-grained sandstone, and (f) mixed sand, shale, and shaly silt from Well Men 105; (g) silty sample with calcite cement, and (h) silt-shale mixture from Well Men 201 (Photographs courtesy of Armel Prosley Mabiala Mbouaki. Copyright 2024).

ensures good hole quality and data integrity. This guarantees a high-quality and dependable interpretation. The overall weighted pay values for well MEN-102 are as follows: Phi = 0.126; Sw = 0.261; HPhiSo = 7.29m. The reservoir consists of numerous thick sandy layers with better properties compared to other Mengo wells. However, the overall reservoir quality remains somewhat poor despite being solely oil-bearing.

This well is situated on the northwestern flank of the Mengo reservoir and serves the purpose of structural appraisal. However, it is heavily affected by borehole enlargement and rugosity. The entire well is predominantly composed of thin laminated sand layers intercalated with shale, leading to challenges in accurately reading parameter values due to the low resolution of the logs. In such a highly shaly environment, the interpretation results are greatly affected and less reliable. Only a few locations, specifically at 1965m/TVD, 1985m/TVD, 2022m/TVD, and 2045m/TVD, show relatively reasonable porosity values of around 9%. Based on these selected points, the overall weighted pay values are as follows: Phi = 0.085. Sw = 0.42. HPhiSo = 7.29m. Despite being the

https://doi.org/10.1021/acsomega.4c08491
ACS Omega 2025, 10, 10081−10106

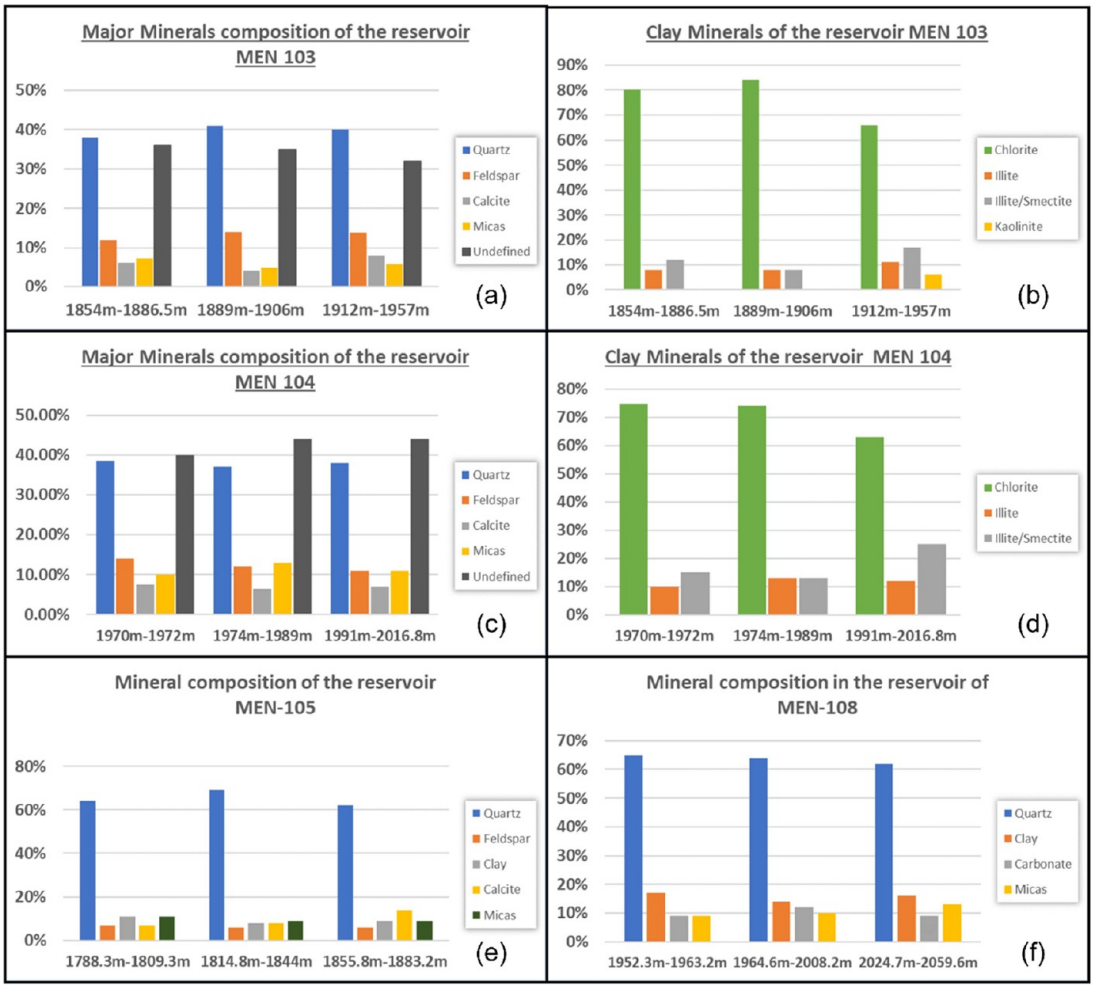

Figure 13. Mineralogical composition of the Mengo sandstone reservoir across four wells. (a) depicts major minerals in well MEN 103, while (b) highlights a high proportion of chlorite among clay minerals in the same well. (c) and (d) illustrate nonclay and clay mineral distributions in well MEN 104, respectively. (e) and (f) demonstrate the dominance of quartz in wells MEN 105 and MEN 108.

most shaly well in this study, the estimated Vclay is only 0.23%, even lower than the cleanest well in the Mengo area (MEN-105). This defies the expectation of Vclay being more than 40%.

In addition, the neutron-density cross-plot analysis was conducted for four wells: MEN-103, MEN-104, MEN-105, and MEN-108. The results reveal that the majority of data points fall within or close to the limestone region on the cross-plots (Figure 11), despite the reservoir not being limestone in composition. This misalignment suggests the influence of significant shale or argillaceous content in the reservoir, as the high clay volume and associated bound water tend to shift the points toward the limestone trend on the neutron-density scale. The clustering of data in this region reflects the shale-dominated or argillaceous nature of the reservoir, emphasizing the importance of integrating additional data, such as core descriptions and mineralogical analyses, to correctly interpret reservoir lithology and petrophysical properties. This observation underscores the complexities of evaluating shaly sandstone reservoirs and the need for careful calibration of petrophysical models to account for clay effects.

Crossplots are commonly used to assess the accuracy of a model.[18] However, density-neutron cross-plot analysis can be challenging in formations with mixed mineralogies, such as shaly sandstone. This ambiguity is evident in well MEN-105 (Figure 11c), where the formation appears more shaly compared to other wells. Despite this, core analysis and well-logging data show favorable results in terms of porosity, mineralogical composition, and net-to-gross ratio. The density-neutron crossplot is particularly useful for identifying the lithology of clean formations like sandstone, limestone, or dolomite filled with oil or water. In this study, no significant gas effects were observed in any wells except for some plots beyond the sand line in MEN-201, which were attributed to specific factors. In MEN-103, all points fall between the limestone and dolomite lines, leaning toward the shale domain, with one point not beyond the limestone line, indicating lower quartz content. Core data confirm the reservoir is not carbonate, though calcite may be present as cement. Thus, the reservoir is identified as a shaly sandstone with significant clay minerals.

Summary of the Results. The petrophysical model for the Mengo reservoir comprises five main elements: three lithologies (sand, clay, and silt), significant carbonate cement, and two fluids (oil and water). The model was constructed based on log, core, and mineralogical studies. The robustness of the model is evident from the interpretation results. A key finding is the absence of true clean sand reservoirs, as indicated by Vclay values of at least 10%. The wells in the Kundji area exhibit more favorable porosity than those in the Mengo area,

https://doi.org/10.1021/acsomega.4c08491
ACS Omega 2025, 10, 10081−10106

with the highest porosity observed in the coarse to medium sand facies based on core tie sections. Water salinity is critical since none of the wells displays a clear water−oil contact (WOC), and salinity measurements are influenced by production water contamination. Applied corrections may not accurately estimate reservoir water salinity. Uncertainties remain, such as the precise mineralogical composition (XRD) and the lack of in situ stress correction for porosity measurements. Recognizing these uncertainties and potential limitations is essential despite the valuable insights the petrophysical model provides. Table 1 below summarizes the results of the calculated parameters of the reservoir.

4.2. Core Analysis and Description. The detailed core description of the Mengo reservoir reveals a diverse range of poorly sorted lithologies, consisting of both coarse and fine grains (Figure 12). These lithologies were primarily deposited through mass transport, debris flows, and turbidite processes in a deep lacustrine environment. The high sand concentration indicates grain flow turbidity, with clays mainly resulting from mica transformation. On a larger scale, these lithologies form depositional packages with either bulk fining-up or bulk coarsening upward trends. Individual beds within these packages may show a coarsening upward trend on a smaller scale but commonly display a fining upward trend on a decimeter scale, typical of debris flow deposition. Based on the turbiditic facies description by Mutti. E et al.(1992),[14] the core analysis identifies four distinct facies within the Mengo reservoir: channels with an erosive base and fining upward sequence, lobes with a coarsening upward trend without an erosive base, laminated facies with alternating thin beds of sand and shale, and shales deposited during periods of low or no clastic input. Among the five wells studied, MEN-105, being closest to the source, exhibits average petrophysical properties compared to the others due to its location.

Core Lithology Identification. A thorough sedimentological description of the cores was conducted to determine the lithofacies in the Mengo sandstone reservoir, focusing on lithology, granulometry (grain size), sedimentary structures, microfractures, and other relevant features. Core analysis of the studied wells revealed a diverse mineral composition, with quartz as the predominant mineral, followed by clay minerals, feldspar, mica, and carbonate. Each mineral significantly influences the rock's behavior during production. Despite quartz being the dominant mineral, clay minerals and feldspar are notable. The mineralogical composition, shown in histograms (Figure 13), indicates that quartz constitutes less than 70% of the composition in all studied wells. Well MEN-105 has the highest quartz content and the lowest clay content, followed by MEN-108, while wells MEN-103 and MEN have quartz content below 40%.

In addition, the photoelectric factor (PEF) log is an excellent indicator of mineralogy. In well MEN-108, PEF values range between 2 and 3 barns/electron, suggesting that quartz, with a reference PEF value of 1.81 barns/electron, is the major mineral. The presence of kaolinite, smectite-Illite interlayers, or Illite is also indicated, but the absence of chlorite, the most abundant clay mineral in the reservoir with a PEF value of approximately 6 barns/electron, likely accounts for the low clay content and favorable reservoir properties observed. Comprehensive mineralogical analysis of the Mengo sandstone reservoir confirms its shaly nature, with clay minerals making up about 32% of the reservoir. Chlorite dominates the clay content, constituting around 80%, followed by Illite. Core analysis and well logging data reveal no clean zones in any of the studied wells, as supported by lithology cross-plots.

In general, Mengo sandstone has a moderately dominant mineralogical composition, with quartz being the primary mineral, followed by clay minerals, feldspars, micas, and carbonates, as shown in the table below (Table 2). The rock XRD mineralogy of the studied field is presented as histograms in Figure 14.

Table 2. Summary of Whole Rock XRD Mineralogy of Mengo Field

minerals	percentage
quartz	40
plagioclase feldspar	10
potassium feldspar	3
carbonates	7
micas	8
clays	32

A set of minerals was identified in the study area through XRD analysis. The mineralogical composition of the studied wells is reported in Figure 13. The major mineral phases include quartz, micas, feldspar, clay minerals, and calcite. Minor phases include pyrite, phosphate minerals, and anhydrite. The content of clay minerals, such as chlorite, Illite, kaolinite, and mixed-layer Illite-smectite, varies between 9% and 17% in the reservoir zone. The total content of quartz, feldspar, recognizable micas, and carbonate minerals, especially calcite, ranges respectively from 30% to 40%, 10% to 13%, 6% to 11%, and 5% to 8%. The porosity and permeability values were determined through core analysis; the results summary of these five wells of the study are presented in Table 3.

The presence of fractures within the reservoir can account for the higher permeability observed in well MEN 201. The porosity values obtained from core analysis and well logging generally correspond in the five wells, except in MEN 201, where the well logging porosity is higher on average compared to the porosity determined from core analysis.

4.3. Well-Test Analysis. The well-testing analysis of the five wells highlights significant variability in production rates and reservoir performance across zones (Table 4). The results include measurements of oil and gas flow rates, gas-oil ratios (GOR), and associated zones. Notable findings show that MEN-103 exhibited an oil flow rate of 5.5 m^3/day and a gas flow rate of 2000−3000 m^3/day during long-term testing in Zone B, with a GOR of 950 m^3/m^3. MEN-105 demonstrated a high oil flow rate (70 to 15.5 m^3/day) across Zones D and E, with variable GORs. Meanwhile, MEN-104, subjected to short-term tests, showed low oil production rates (25−40 L/hour) in Zone F. These data underscore the heterogeneity of reservoir performance, reflecting the influence of lithological and petrophysical variations on production potential.

4.4. Reservoir Quality. Identifying the type and distribution of clay is crucial due to its significant impact on petrophysical parameters like porosity, permeability, and water saturation. This study used cross-plots of neutron porosity versus density porosity (Figure 11) to characterize the shaly sandstone. The analysis revealed that all five wells exhibit a dispersed clay distribution, which is essential for understanding the properties of the reservoir.

Using neutron-density cross-plots (Figure 11) and histogram distributions (Figure 13), the lithology, mineral composition,

https://doi.org/10.1021/acsomega.4c08491
ACS Omega 2025, 10, 10081−10106

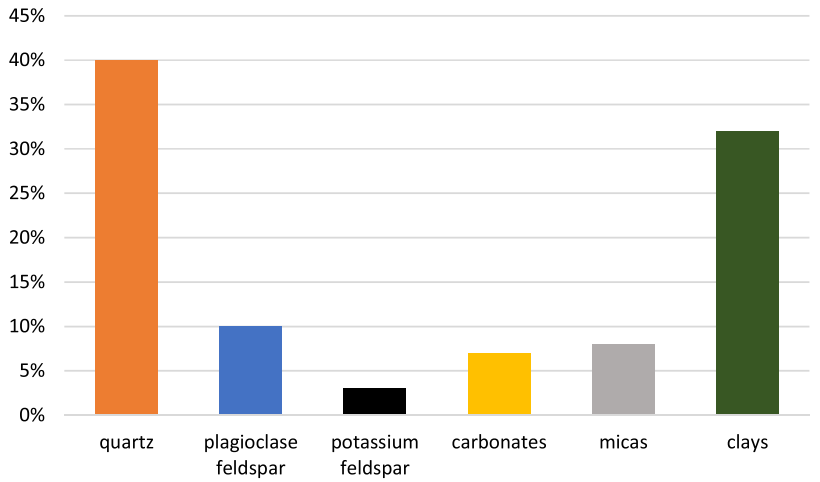

Figure 14. Histogram of rock XRD mineralogy of Mengo field. Overall mineralogical composition of the Mengo sandstone reservoir.

Table 3. Core Porosity and Permeability of Four Studied Wells

	porosity (%)			permeability (mM)		
well	min	ave	max	min	ave	max
MEN-103	2.3	9.81	8.8	0.04	0.29	16.90
MEN-104	1.1	8.4	15.2	0.04	0.19	1.20
MEN-105	2.2	11.0	19.5	0.01	0.16	2.40
MEN-108	2.2	9.6	16.2	0.06	1.13	6.91
MEN-201	2.1	10.06	18	0.04	1.02	10.9

and porosity of the Mengo sandstone reservoir were analyzed, revealing a mixture of shaly lithology with minor carbonate content. Gamma-ray values and porosity measurements across the wells indicate the absence of pure sand. Well MEN-103 has gamma-ray values from 54.39° to 105.22° API and porosity between 1% and 18.57%, while MEN-104 ranges from 43.75° to 103.81° API with 0% to 27% porosity. MEN-105 shows gamma-ray values from 47.75° to 103.68° API and porosity from 1% to 20.1%. MEN-108 exhibits gamma-ray values from 52.88° to 100.22° API with porosity between 0% and 29%, and MEN-201 has gamma-ray values from 54.03° to 113.37° API with 0% to 18.57% porosity. The consistent high gamma-ray readings confirm the lack of pure sand throughout the reservoir.

The Mengo shaly sandstone reservoir exhibits moderate to favorable reservoir quality across its wells. Well MEN-105 has a net pay thickness of 77.61 m, an average effective porosity of 12.3%, a clay volume of 26.6%, and a hydrocarbon saturation of 60.60%. Well MEN-103 features a producible shaly sand zone with a net pay thickness of 50.6 m, an average porosity of 12.8%, a hydrocarbon saturation of 58%, and a shale volume of 20.5%. Well MEN-104 has a net pay thickness of 22.86 m and a hydrocarbon saturation of 59.2%, while MEN-108 shows a net pay thickness of 65.11 m, a hydrocarbon saturation of 60%, and a shale volume of 25.5%. Well MEN-201 has a net pay thickness of 37.38 m, an average effective porosity of 16.9%, a hydrocarbon saturation of 60.4%, and a shale volume of 28.8%. Overall, the average petrophysical properties for the wells range from 22.86 to 77.61 m in net pay thickness, 10.5% to 16.9% in effective porosity, 20.5% to 28.8% in shale volume, 39.4% to 42% in water saturation, and 58% to 60.6% in hydrocarbon saturation.

5. DISCUSSION

This investigation analyzed well logging responses to understand how clay minerals influence the petrophysical characteristics of the Mengo shaly sandstone reservoir. The objective was to identify the processes affecting the pore system properties in this shaly sandstone formation.

5.1. Clay Mineral Diagenesis and the Influence of Other Minerals on Reservoir Quality. The petrophysical properties of shaly sandstone reservoirs, such as porosity, permeability, and fluid saturation, are significantly influenced by clay minerals and other diagenetic minerals. Studies reveal a strong relationship between clay content and reservoir quality, with higher clay volumes generally reducing porosity and permeability.[19] Core analysis of the Mengo shaly sandstone reservoir shows it comprises 40% quartz, 32% clay minerals, 13% feldspar, 8% mica, and 7% carbonate. While quartz is the

Table 4. Well-Testing Results of the Five Studied Wells

well name	test type	oil flow rate	gas flow rate	gas-oil ratio	zone
MEN-103	long-term	5,5 m^3/day	2000 to 3000 m^3/day	950 m^3/m^3	B
		1−2 m^3/day			
MEN-104	short-term	25 l/h, 37 l/h, 40 l/h			F
MEN-105	long-term	70 to 15,5 m^3/day		177 to 458 m^3/m^3	D
		73 to 15 m^3/day		120 to 449 m^3/m^3	F
MEN-108	short-term	1,7m^3 oil + water/10 h			F
		8171 oil + water//12 h 30			D
MEN-201	long-term after fracking	5 m^3/day			
		4 m^3/day			

https://doi.org/10.1021/acsomega.4c08491
ACS Omega 2025, 10, 10081−10106

most abundant mineral, each mineral present influences the reservoir's behavior, particularly during production.

In the Mengo shaly sandstone reservoir, high clay mineral content can reduce porosity and permeability, impacting production. Chlorite is the most dominant clay mineral, followed by Illite/Illite-smectite, with very few kaolinites. Each clay mineral affects the reservoir differently. Mineralogical data (Figure 13), well logging data (Table 1), and well test data (Table 4) indicate that wells MEN-105 and MEN-108 have the best petrophysical properties due to their lower clay content compared to other wells. This demonstrates a correlation between reservoir quality and clay content in the Mengo shaly sandstone reservoir, suggesting that clay content significantly influences porosity, permeability, saturation, and hydrocarbon recovery.

5.1.1. Chlorite. Chlorite ($Al_2O_32SiO_22H_2O$) is the most dominant clay mineral in the Mengo reservoir and significantly impacts the shaly character of the formation. This mineral, featuring a tetrahedral-octahedral structure, originates from alterations of odinite, berthierine, and smectite or from the dissolution of Fe- and Mg-rich detrital grains. Fe-rich chlorite coatings reduce pore throat size, increase microporosity, and lower permeability, negatively affecting reservoir quality by forming clay bridges and pore-filling cements that impede fluid flow.[20] Chlorite coatings on detrital grains can also act as barriers to fluid flow, significantly reducing hydrocarbon recovery and increasing water retention.[21,22] Chlorite's influence extends to well productivity, as it contributes to clay swelling and impacts the reservoir's response to stimulation treatments like hydraulic fracturing and acidizing.[23] Chlorite coatings in deeper sandstone reservoirs, however, can have a stabilizing effect by preserving primary intergranular porosity from compaction and inhibiting quartz overgrowth, which reduces nucleation.[24,25] While this protection can enhance reservoir quality, excessive authigenic chlorite may fill reservoir space, further reducing porosity.[25,26] The overall impact of chlorite in the Mengo reservoir highlights the complex role this mineral plays in influencing porosity, permeability, and hydrocarbon recovery.

5.1.2. Illite. Illite with the chemical formula (K,H_3O)-$(Al,Mg,Fe)_2(Si,Al)_4O_{10}[(OH)_2(H_2O)]$, is another key clay mineral present in the Mengo reservoir, ranking as the second most abundant clay mineral. Its small, fibrous, and complex crystals are known to clog pore throats, thereby reducing permeability. Illite's morphology varies, with hairy, fibrous, and ribbon-like forms often coating rock surfaces, narrowing pores and further reducing permeability.[27] In addition to pore clogging, fibrous Illite exposed to water or shear stress can fragment, migrate, and block capillaries, further limiting fluid flow. Illite can also act as a pore-filling cement, diminishing both porosity and hydrocarbon production potential.[28,29] High Illite content typically results in shaly sandstones with reduced permeability and increased irreducible water saturation, which hampers hydrocarbon recovery.[30] Moreover, Illite's role in diagenetic transformation affects reservoir quality by altering the pore structure and influencing production dynamics.[31,32] Its obstructive effects on pore throats make Illite a significant factor in shaping the Mengo reservoir's petrophysical properties.

5.1.3. Kaolinite. Kaolinite, with the chemical formula $Al_2O_32SiO_22H_2O$, although less abundant in the Mengo reservoir and primarily observed in well MEN-103, also impacts porosity and permeability. Typically formed through the dissolution of feldspar, kaolinite influences fluid flow and hydrocarbon recovery in shaly sandstone reservoirs due to its high surface area and cation exchange capacity.[33,34] Kaolinite's presence can reduce rock strength and increase deformation, while also affecting wettability and oil recovery through its role in hydrocarbon retention and ion exchange.[35] Understanding kaolinite's impact is essential for optimizing production strategies in clay-rich reservoirs.

5.1.4. Feldspar. Feldspar, comprising 13% of the Mengo reservoir, plays a unique role due to its potential for diagenetic transformation into clay minerals, such as kaolinite, under chemical weathering. While feldspar dissolution can increase porosity by creating secondary dissolution pores, these pores may be isolated and lack connectivity, thus having a minimal contribution to permeability.[36−38] Additionally, feldspar dissolution may release ions that precipitate other clay minerals, such as kaolinite, chlorite, and Illite, which can clog pore spaces and further reduce permeability.[2,38−40] Consequently, feldspar's presence contributes to mineralogical heterogeneity and influences reservoir quality through its transformation into secondary minerals, which can modify wettability and fluid flow properties.[41]

5.1.5. Micas. Micas, comprising 8% of the mineral composition in the Mengo reservoir, also impact reservoir quality through their roles as cementing and pore-filling minerals. As they undergo alteration, micas can affect the mechanical strength, fluid storage capacity, and production rates by influencing fluid connectivity and pore structure[42,43] Additionally, their presence affects porosity and permeability, as well as the overall behavior of fluid flow in shaly sandstone reservoirs.[44,45] Micas' ability to alter petrophysical properties and reservoir behavior underscores their significance in reservoir quality assessments.

Together, these minerals chlorite, Illite, kaolinite, feldspar, and micas—highlight the importance of a detailed mineralogical and diagenetic understanding of the Mengo shaly sandstone reservoir. Chlorite and Illite, as dominant clay minerals, significantly reduce permeability and reservoir quality, with chlorite affecting fluid flow through coating formation and Illite impacting pore connectivity. Kaolinite, although less common, contributes to hydrocarbon retention and rock deformation. Feldspar and micas, through their diagenetic transformations, further influence reservoir heterogeneity, porosity, and permeability. This combined analysis underscores the necessity of mineralogical and petrophysical evaluations in optimizing hydrocarbon recovery strategies in clay-rich sandstone reservoirs.

5.1.6. Clay Mineral Effects on Wellbore Stability, Water Saturation, Capillary Pressure, and Compressibility. The presence of clay minerals can have implications for wellbore stability. These minerals have the potential to expand, which can result in wellbore instability and give rise to issues such as pipe blockage, borehole collapse, and poor circulation. Research conducted by Rassool et al. (2023)[46] has highlighted the significant impact of smectite clay minerals on wellbore stability, necessitating appropriate drilling fluid design and management practices.[46] Furthermore, clay minerals can influence the geomechanical properties of a reservoir. They can increase its susceptibility to compaction, leading to subsidence or deformation of the overlying strata.[6] Additionally, clay minerals can exhibit sensitivity to changes in temperature and pressure, causing them to expand or contract.

https://doi.org/10.1021/acsomega.4c08491
ACS Omega 2025, 10, 10081−10106

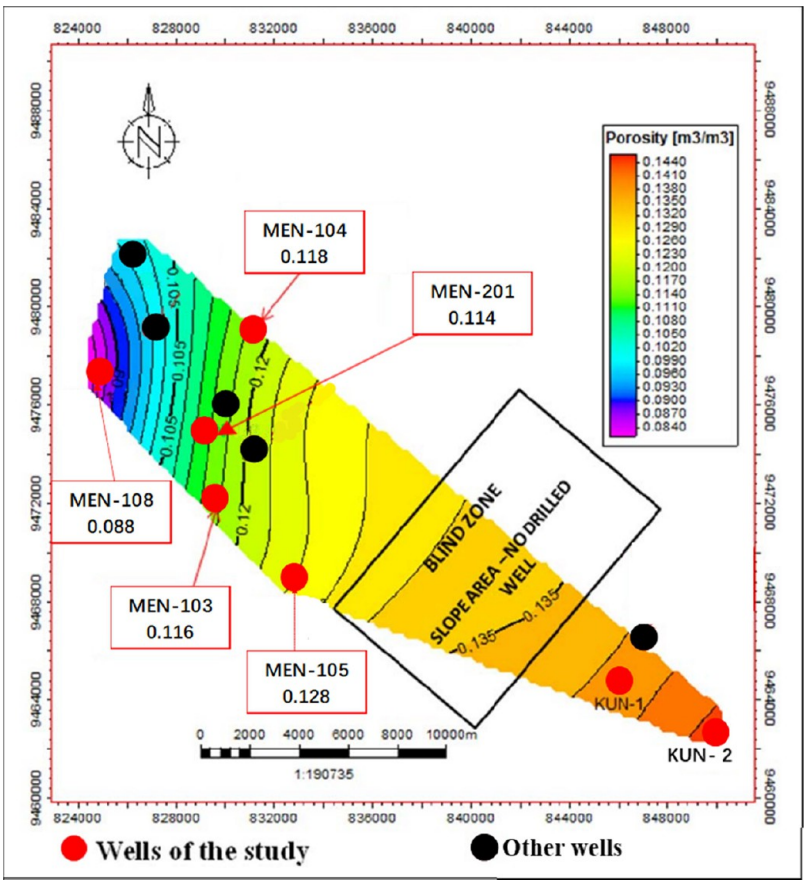

Figure 15. Porosity distribution map of the Mengo Shaly Sandstone Reservoir. Warmer colors (yellow to red) indicate higher porosity, while cooler colors (blue to green) represent lower porosity. The blind zone and slope area, where no wells are drilled, highlight a structural or stratigraphic transition with distinct porosity characteristics.

These changes in volume can alter the stress state of the reservoir[47]

Clay minerals also play a role in influencing the water saturation of shaly sand reservoirs. These minerals have the ability to increase water saturation by adsorbing water molecules onto their surfaces. According to research conducted by Bahrami et al. (2015),[48] clay minerals can increase water saturation by up to 16%.[48] Higher levels of water saturation can impede hydrocarbon migration and slow production rates. Furthermore, the presence of clay minerals can alter the wettability of shaly sand reservoirs. The composition of clay minerals within a formation can determine whether it exhibits water-wet or oil-wet characteristics. Studies have indicated that shaly sandstones containing Illite, chlorite, and smectite clay minerals are more likely to exhibit water-wet behavior compared to those containing kaolinite clay minerals.[49,50]

Clay minerals can indeed affect the compressibility of a shaly sand reservoir, potentially making it more compressible and impacting its fluid storage capacity. This is particularly true when the formation contains significant clay minerals. Research conducted by Tiwari et al. (2011)[51] has established a positive correlation between the presence of clay minerals and the compressibility of a formation. Furthermore, clay minerals in a reservoir, such as the Mengo sandstone, can influence the capillary pressure of a reservoir. Capillary pressure is the difference required to displace fluids from the pore spaces within a formation. The presence of clay minerals, which can trap fluids in the pore spaces, can increase the capillary pressure of a formation. Zhao et al. (2018)[52] have conducted research demonstrating that the quantity and type of clay minerals in a reservoir can significantly impact its capillary pressure.

5.1.7. Effect of Clay Minerals on Fluid Flow. The presence of clay minerals can fill void spaces, thereby reducing the total porosity. The type and amount of clay minerals present in the reservoir primarily control porosity. Depending on their morphology and distribution within the reservoir, different types of clay minerals can have varying impacts on porosity. Permeability is also affected by clay minerals, the presence of these minerals can reduce permeability, making it more difficult for fluids to flow through the reservoir.[2] This is because clay minerals can block or reduce the size of the pathways through which fluids flow.[53,54] The impact on permeability can be influenced by the type of clay mineral and its distribution within the reservoir.[55,56] The presence of clay minerals can also affect the production rate from a reservoir. This is because the reduction in porosity and permeability caused by clay minerals can lower the reservoir's ability to store and transmit fluids, thereby affecting the rate at which hydrocarbons can be produced.[57] Additionally, clay minerals can add electrical conductivity to the formation, leading to overestimating water saturation using conventional clean sand approaches. This can result in bypassed production as these zones may be considered non commercial.[57]

5.2. Porosity and Permeability. The average effective porosity in the oilfield ranges from 8.8% in well MEN-108 to

https://doi.org/10.1021/acsomega.4c08491
ACS Omega 2025, 10, 10081−10106

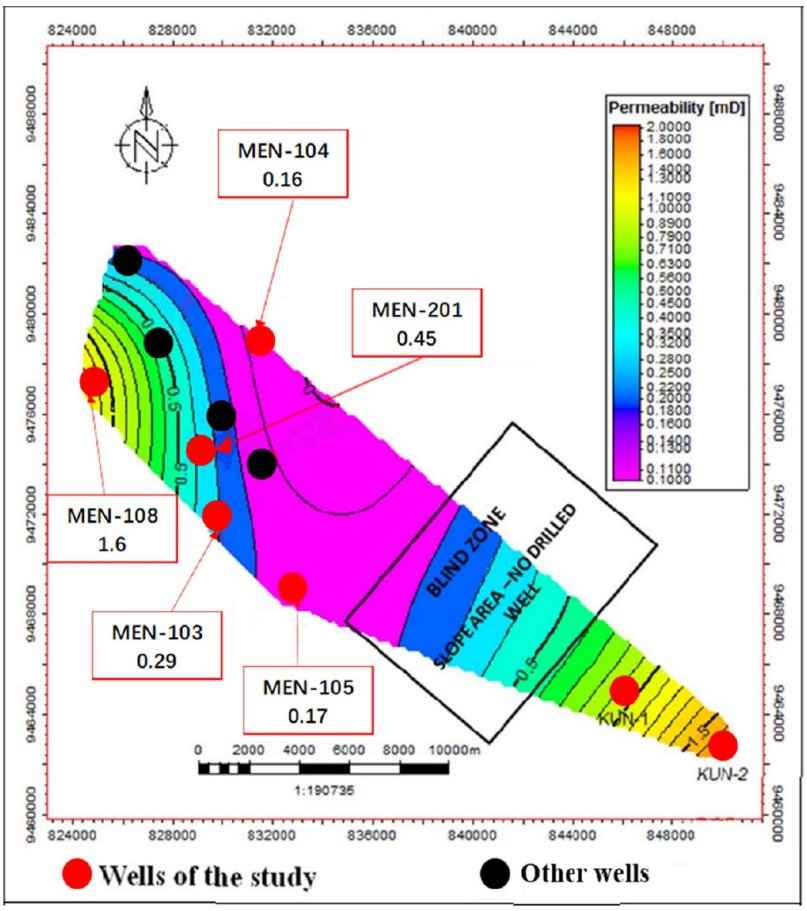

Figure 16. Mengo Shaly Sandstone Reservoir's distribution Map of permeability, Warmer colors (yellow to red) indicate zones of higher permeability, while cooler colors (purple to blue) represent lower permeability. A blind zone and slope area, where no wells have been drilled, are highlighted, indicating a structural or stratigraphic transition zone with unique permeability characteristics distinct from the surrounding regions.

12.8% in well MEN-105. While vertical variation within each well is minimal, there is a noticeable lateral decrease in porosity from the Kundji area to the Mengo area, as shown in Figures 15 and 16. This trend aligns with the geological model, which suggests higher porosity near the sediment source in the Kundji area due to its proximity to sediment supply from the southeast to the northwest and lower porosity in the distal Mengo area. Additionally, reservoir texture influences this pattern, with coarse to very coarse sand containing some pebbles exhibiting better porosity than fine-grained sand. This is the fact that quartz grains in coarse sand have increased fissuration related to their grain size.

The coarse to conglomerate facies (F1 to F5) described by Mutti et al. (1992),[14] indicative of debris flows and high-density turbidites, are prevalent in the Kundji area. However, in the Mengo area, these facies are only observed in the proximal parts of the lobes, particularly in well MEN-105. Detailed examination of thin sections reveals advanced diagenesis features associated with dominant secondary porosity. The reservoir contains various postlithification fractures filled with calcite (patchy pore-filling carbonate cement) or clay. This suggests that the poor reservoir quality cannot be attributed solely to the depositional environment. Given our limited understanding of the environment, diagenetic processes must also be considered. These include early lithification, the disintegration of clays (coating and pore-filling authigenic chloritic and illitic clays), micas, and organic-rich clay clasts within the sandstones, as well as the presence of authigenic clays and carbonate cements, and the dominance of secondary porosity.,

The analysis of core samples indicates the presence of uncemented, poorly consolidated organic-rich shales, likely due to methane preventing diagenetic alteration. Methane expulsion has created fissures and fluidized features, known as stress release structures, within the reservoir. Scanning Electron Microscope (SEM) images (Figure 17, 18, 19 and 20) reveal the obstructive impact of calcite and diagenetic chlorite on pore throat connectivity. Clay minerals act as natural adhesives, reducing permeability by filling gaps between sand grains and forming a matrix that decreases interconnected pore space, complicating fluid flow. This significantly impacts oil

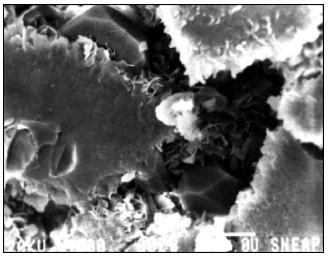

Figure 17. SEM photo showing authigenic calcite and diagenetic chlorite obstructing pore throat connections in Kundji area (KUN 1, 1435m).

https://doi.org/10.1021/acsomega.4c08491
ACS Omega 2025, 10, 10081−10106

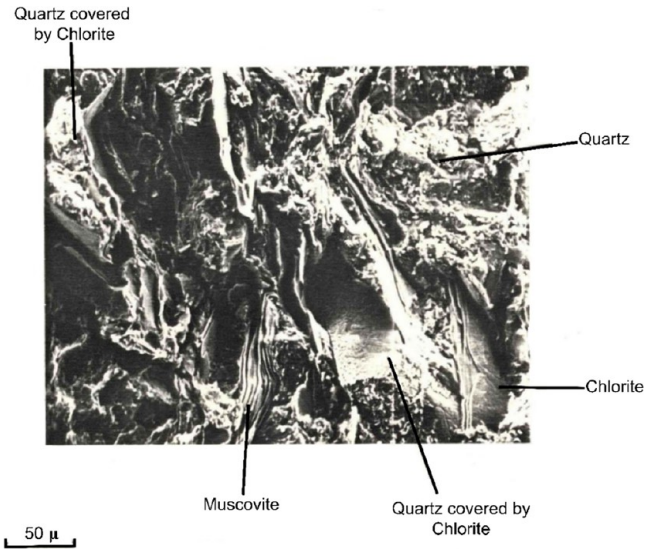

Figure 18. Mineral composition and texture within a MEN-108 sample displayed in SEM image, highlighting key minerals in a chlorite-rich matrix. Several quartz grains are observed, with chlorite coatings, indicating postdepositional chloritization, which can influence the porosity and permeability of the reservoir.

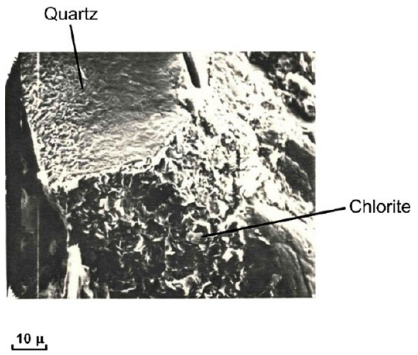

Figure 19. SEM image showcasing the mineralogical features of a sample, with quartz and chlorite identified through energy-dispersive X-ray analysis (EDAX). Chlorite is prominently observed as pore-filling cement, contributing to secondary porosity reduction and significantly impacting fluid flow properties within the reservoir.

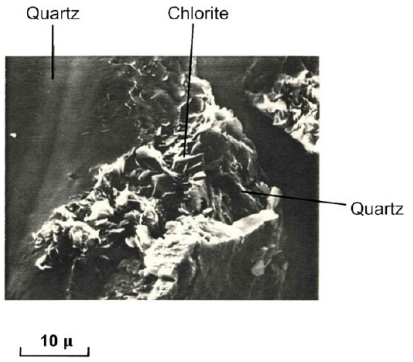

Figure 20. SEM photograph displaying a close-up view of the mineralogical composition in a sample, specifically showing quartz and chlorite. Chlorite is seen partially covering and interacting with the quartz grains, suggesting potential impacts on porosity and permeability, as it often precipitates within pore spaces, thereby reducing pore connectivity.

and gas production capabilities in shaly sand reservoirs. Clay particles, being less than 2 μm in size, further reduce porosity and permeability. Vasconcelos et al.(2016)[58] found that clay minerals can decrease reservoir permeability by 10−20%, while Golsanami et al.(2022)[59] demonstrated reductions in porosity and permeability by over 30% and 400mD, respectively. Additionally, reported clay minerals could decrease porosity by up to 12% and permeability by up to 86%.

The permeability values are disproportionately low compared to the corresponding porosity values, indicating a lack of correlation between the two parameters. Despite having the lowest porosity in the Mengo area, well MEN-108 is surprisingly the most permeable. This reservoir, heavily influenced by diagenesis, exhibits three types of porosity, each with distinct permeability characteristics. Dissolution porosity has negligible permeability due to isolated pores, while intergranular permeability is reduced by chlorite and Illite coatings. Fissuration permeability, developed through methane-induced hydrofracturing, is prominent in low Net to Gross areas like MEN-104 and MEN-201. Well tests in fissured layers E and F of KUN-1 show significant permeability enhancement from fissures.

Additionally, natural permeability processes contribute to high productivity in the MKB reservoir despite low permeability (1.5 MMBO of 32 API waxy oil), as methane-filled fractures help transport oil, as demonstrated by Nunn and Meulbroek. Core permeability measurements vary from negligible to poor, with averages from 0.16 mD (MEN-104) to 1.68 mD (KUN-2) and maximum values from 0.77 mD (MEM-101) to 75.5 mD (KUN-1). These values are generally low compared to porosity, yet wells like MEN-108 with poor core porosity still exhibit high permeability. A detailed analysis of core permeability revealed that many cores near fissured zones were broken, indicating high fissuration that was not accounted for in permeability measurements. Consequently, the permeability map primarily reflects intergranular and low to average fissuration permeability, neglecting the highly fissured zones. This explains why well MEN-10, despite being a top producer in a highly fissured area, shows low permeability on the map, as only its intergranular permeability is considered. Additionally, low permeability can be attributed to factors such as a high proportion of fine grains combined with poor sorting, the presence of angular to subangular grains, a high amount of easily altered mica grains mixed with fine grains leading to strong compaction of the sandstones, and significant clay content obstructing pore throats.

The presence of clay minerals in shaly sand reservoirs significantly reduces porosity and permeability, hindering fluid flow and lowering production rates.[32,53] Due to their small particle size, clay minerals can fill pore spaces and obstruct fluid movement.[54] The type and amount of clay minerals present greatly influence the impact on porosity. For instance, Iranfar et al.(2023)[60] found that Illite and kaolinite clays more severely reduce porosity than smectite clays. Consequently, the presence of these minerals acts as a barrier, with permeability loss being directly proportional to their type and quantity in the formation.

5.3. SEM Analysis of the Mengo Shaly Sandstone Reservoir. SEM analyses (Figures 17 to 20) of the Mengo shaly sandstone reservoir provided critical insights into the influence of mineralogical and diagenetic processes on reservoir quality. In the Kundji area (KUN-1, 1435m), SEM imaging revealed authigenic calcite and diagenetic chlorite

https://doi.org/10.1021/acsomega.4c08491
ACS Omega 2025, 10, 10081−10106

obstructing pore throat connections, illustrating the role of postdepositional mineralization in reducing permeability. In MEN-108 samples, a chlorite-rich matrix with quartz grains coated by chlorite was observed, indicating significant postdepositional chloritization. These chlorite coatings are known to restrict pore connectivity and adversely affect fluid flow, emphasizing their importance in determining reservoir performance.

Energy-dispersive X-ray analysis (EDAX) further highlighted quartz and chlorite as dominant minerals within the reservoir. Chlorite was frequently observed as pore-filling cement, reducing secondary porosity and blocking pore spaces, a key factor in permeability reduction. Additionally, chlorite's interaction with quartz grains, as seen in close-up SEM images, demonstrated its tendency to precipitate within pore spaces, compounding the reduction in pore connectivity. These findings underscore the need for detailed mineralogical assessments to better understand and address the impact of diagenetic processes on porosity and permeability during reservoir evaluations.

Additionally, X-ray diffraction (XRD) mineralogy data show minimal calcite presence, so it was excluded from interpretation. The analysis reveals three porosity types in the MKB field: dissolution porosity, intergranular porosity, and fissuration porosity. Dissolution porosity, caused by feldspar dissolution, is the dominant type in all wells, but it consists mainly of poorly connected isolated pores. Intergranular porosity, reduced by neoformation clays like chlorite and Illite, and fissuration porosity, created by hydro-fracturing from methane in organic shale, contribute to better permeability. Despite being the least common, fissuration porosity is highly developed in low Net to Gross areas due to high methane content (e.g., MEN-102, MEN-108). Reservoir quality interpretation should account for diagenesis, as porosity measured from logs includes all three types, with only intergranular and fissuration porosities linked to good permeability.

5.4. Reservoir Quality Prediction through Petrophysical Modeling. The prediction of reservoir quality in the Mengo Shaly Sandstone Reservoir involves comprehensive petrophysical modeling using various well-logging and core data to estimate porosity, permeability, fluid saturation, and clay volume. The integration of gamma-ray, density, neutron, resistivity, and sonic logs allows the assessment of lithology and quantification of shale content, crucial for understanding the reservoir's quality in shaly sandstone environments. By calibrating these log interpretations with core data, including porosity and permeability measurements, a robust predictive model is developed.

Porosity and Permeability Prediction. The effective porosity and permeability were estimated using petrophysical evaluation and cross-plot methods that incorporate density-neutron and sonic-neutron porosity relationships, with further adjustments for shale volume through gamma-ray readings. The model's predictive accuracy was enhanced by applying effective porosity and shale volume cutoffs to identify potential zones for hydrocarbon accumulation. Permeability estimates were further refined using a combination of core-derived porosity-permeability relationships and well-log transformations, accounting for clay-induced heterogeneity.

Water Saturation and Hydrocarbon Saturation. Using the Indonesian method for water saturation, particularly relevant in clay-rich reservoirs, enabled more accurate estimates in the Mengo reservoir. This approach factors in the clay-bound water, providing more reliable hydrocarbon saturation predictions. Through this petrophysical modeling, the reservoir's net pay zones, effective porosity, and hydrocarbon saturation distribution can be mapped, identifying key zones of interest for future production.

Model Validation and Calibration. Calibration with core data has confirmed the reliability of the petrophysical model, as evident in the correlation between log-based and core-based porosity and permeability. This calibrated model thus enables reliable predictions of reservoir quality, which can guide field development strategies in the Mengo reservoir.

5.5. Controlling Factors and Demarcation of Favorable Zones of Sand Accumulation. The distribution and quality of sand bodies in the Mengo shaly sandstone reservoir are influenced by several key geological and diagenetic factors that control reservoir quality. Understanding these controlling factors is essential to identifying zones with favorable sand accumulation and improved reservoir properties.

Primary Controlling Factors. Depositional Environment. The Mengo reservoir's sandstones were deposited in a lacustrine to deltaic environment, where mass transport and debris flows influenced the texture and sorting of sediments. The fan-shaped depositional system has led to variable grain sizes, with coarser sands generally found in the proximal regions, particularly around the midfan area.

Clay Mineral Distribution. The high clay content, particularly chlorite and Illite, has a significant impact on the reservoir's porosity and permeability. Clay minerals tend to reduce pore throat size, leading to reduced permeability. Zones with lower clay concentrations, such as those around well MEN-105, are identified as more favorable for sand accumulation.

Diagenetic Overprint. Diagenetic processes, including chlorite cementation and quartz overgrowth, further modify porosity and permeability. While chlorite coatings can preserve porosity by inhibiting quartz overgrowth, excessive chlorite content reduces permeability by clogging pore spaces.

Demarcation of Favorable Zones. By mapping the porosity, permeability, and net-to-gross thickness across the field, the midfan region centered around well MEN-105 emerges as the most promising area for sand accumulation and hydrocarbon extraction. This zone benefits from a relatively high net-to-gross ratio, moderate to high porosity, and the presence of fissures induced by methane gas, which enhances fissural permeability. The upper to midfan area around MEN-105 is identified as a priority for future drilling, as it combines favorable porosity and a dense network of fissures, contributing to increased hydrocarbon mobility despite the low intergranular permeability.

5.6. Reservoir Quality Assessment and Optimal Zone Identification. In evaluating the best reservoir area, all reservoir quality parameters, including porosity, permeability, net pay, and net to gross, should be integrated.[7,9] The net-to-gross value confirms that well MEN-105 is the most proximal well in the Mengo area, with the highest net-to-gross ratio in the entire field, followed by well MEN-103. On the other hand, wells MEN-201 and MEN-104 have the lowest net-to-gross values for this parameter. Based on the net pay values, well MEN-105 remains the best well among the five wells analyzed in the field. The combination of overall parameters allows us to rank the areas as follows: The midfan area of the Mengo region centered around well MEN-105, is considered the best zone.

https://doi.org/10.1021/acsomega.4c08491
ACS Omega 2025, 10, 10081−10106

This zone benefits from a dense network of fissures and a high methane content, resulting in a fissuration permeability while the normal permeability is low. The well MEN-105 is the best in the entire Mengo area, and the upper to midfan area surrounding well MEN-105 is chosen for its superior H.Phi. However, the permeability in this area is very low, necessitating the implementation of artificial enhancement methods.

From both porosity and permeability values, it can be observed that the most porous wells are not necessarily the most permeable, particularly in the Mengo area. Surprisingly, the less porous well (MEN-108) appears to be the most permeable one (Figure 18 and Figure 19). Thus, permeability depends on the type of porosity: Porosity from fissures is associated with very good permeability;[61−63] Intergranular porosity is linked to good permeability if the pore throats are not reduced or plugged;[64,65] Porosity from dissolution is associated with negligible permeability because the pores are mainly isolated.[66,67] In such a complex environment, relying solely on log porosity which is unable to discriminate between the different porosities, is deceitful.

6. CONCLUSION

The Mengo reservoir, consisting of poorly sorted coarse and fine-grained lithologies, was deposited through mass transport, debris flows, and turbidites within a deep lacustrine environment. Its complex geology necessitated the integration of logs and core data into a conceptual geological model to understand petrophysical parameter distribution and identify prospective zones. However, interpretation challenges arose due to high radioactivity, mica and feldspar abundance, lack of clear water zones for Rw calculation, absence of clean zones for cutoff parameters, high clay volume (~25%), and low permeability (average <2 mD).

Despite these obstacles, the petrophysical model showed strong reliability, correlating well with core data. It identified five key components: three lithologies (sand, clay, and silt) and two fluids (oil and water). No Oil−Water Contact (OWC) was observed across the five studied wells, underscoring water salinity's role in reservoir evaluation. Porosity ranged from moderate to good (8%-15% per well), while permeability was consistently low, averaging between 0.16 mD (Mengo-104) and 1.68 mD, with diagenesis and clay content as major limiting factors.

The study underscores that high clay content in sandstone reservoirs can render them unproductive, as demonstrated by the Mengo reservoir's abandonment. Focus has shifted to fissuration permeability and reservoir quality parameters (Net-to-Gross, Net Pay, and porosity) to identify optimal zones for future drilling. The midfan area near MEN-105 emerged as the most favorable location for future wells. Estimating permeability remains difficult without distinguishing porosity types, emphasizing the need for detailed analysis of porosity distribution and its role in diagenesis-affected permeability at the field scale. The most porous well is not necessarily the most permeable; permeability depends on the porosity type.

AUTHOR INFORMATION

Corresponding Author

Armel Prosley Mabiala Mbouaki − *Key Laboratory of Theory and Technology of Petroleum Exploration and Development in Hubei Province and Key Laboratory of Tectonics and Petroleum Resources Ministry of Education, China University of Geosciences, Wuhan 430074, China*; orcid.org/0009-0001-6720-8442; Email: prosleymab@gmail.com

Authors

Zhongxian Cai − *Key Laboratory of Theory and Technology of Petroleum Exploration and Development in Hubei Province and Key Laboratory of Tectonics and Petroleum Resources Ministry of Education, China University of Geosciences, Wuhan 430074, China*

Elia Wilinasi Sikanyika − *Key Laboratory of Theory and Technology of Petroleum Exploration and Development in Hubei Province and Key Laboratory of Tectonics and Petroleum Resources Ministry of Education, China University of Geosciences, Wuhan 430074, China*

Grant Charles Mwakipunda − *Key Laboratory of Theory and Technology of Petroleum Exploration and Development in Hubei Province and Key Laboratory of Tectonics and Petroleum Resources Ministry of Education, China University of Geosciences, Wuhan 430074, China*

Hugues Roland Konan − *Key Laboratory of Theory and Technology of Petroleum Exploration and Development in Hubei Province and Key Laboratory of Tectonics and Petroleum Resources Ministry of Education, China University of Geosciences, Wuhan 430074, China*

Complete contact information is available at: https://pubs.acs.org/10.1021/acsomega.4c08491

Notes

The authors declare no competing financial interest.

ACKNOWLEDGMENTS

The authors express their appreciation to the Congolese National Petroleum Company (SNPC), the Chinese Government scholarship (CSC), and the Department of Petroleum Engineering of China University of Geosciences-Wuhan.

NOMENCLATURE

Roman symbols	Meaning
a	Tortuosity exponent
c & b	Constants based on the K-transform group, effective porosity and shale volume
Eq	Equation
GR_{index}	Gamma ray index
GR_{matrix}	Gamma matrix
GR_{shale}	Gamma ray in shale
k	Permeability in md
m	Cementation exponent
n	Saturation exponent
R_{MF}	Mud filtrate resistivity
R_o	Resistivity of oil
R_{sh}	Resistivity log reading in 100 shale
R_t	Formation resistivity
R_w	Water resistivity
T_{MF}	Mud filtrate temperature
ϕ	Effective porosity (v/v)
Φ_n	Neutron porosity
Φ_d	Density porosity
ρ_b	Bulk density
ρ_{lim}	Limestone grain density
ρ_{mf}	Mud filtrate density
ρ_{sand}	Sandstone grain density
ρ_{dol}	Dolomite grain density

https://doi.org/10.1021/acsomega.4c08491
ACS Omega 2025, 10, 10081−10106

ABBREVIATION LONGFORM

BLI	Bottom Log Interval
BLT	Bottom Log Temperature
CAL	Caliper
CEC	Cation Exchange Capacity
SNPC	Congolese National Petroleum Company
DEN	Density
FTEMP	Formation temperature
GR	Gamma Ray
GOR	Gas Oil Ratio
MD	Measured Depth
MMBO	Million barrel of oil
NPHI	Neutron
OWC	Oil–Water Contact
OBM	Oil-Based Mud (OBM)
PHIE	Effective Porosity
PHIT	Total Porosity
ROS	Residual Oil Saturation
TLI	Top Log Interval
TLT	Top Log Temperature
TVD	True Vertical Depth
TVDSS	True Vertical Depth Sub Sea
Vclay	Clay Volume
Vsh	Shale Volume
XRD	X-ray Diffraction

REFERENCES

(1) Pitt, H.; Rutkowski, E.; Larsen, K. *Fueling a Transition Away from Fossil: The Outlook for Global Fossil Fuel Demand*. 2024.

(2) Al-Kharra'a, H. S.; Wolf, K.-H. A. A.; AlQuraishi, A. A.; Mahmoud, M. A.; Deshenenkov, I.; AlDuhailan, M. A.; Alarifi, S. A.; AlQahtani, N. B.; Kwak, H. T.; Zitha, P. L. J. Impact of Clay Mineralogy on the Petrophysical Properties of Tight Sandstones. *Geoenergy Sci. Eng.* **2023**, *227*, No. 211883.

(3) De, S.; Varma, A. K.; Sengupta, D. Recent Advances in Well Logging Techniques for Exploration of Shale Reservoirs. *Unconv. Shale Gas Explor. Exploit. Curr. Trends Shale Gas Exploit.* **2024**, 49–67.

(4) Ehsan, M.; Gu, H. An Integrated Approach for the Identification of Lithofacies and Clay Mineralogy through Neuro-Fuzzy, Cross Plot, and Statistical Analyses, from Well Log Data. *J. Earth Syst. Sci.* **2020**, *129*, 1–13.

(5) Shedid, S. A. A New Technique for Identification of Flow Units of Shaly Sandstone Reservoirs. *J. Pet. Explor. Prod. Technol.* **2018**, *8*, 495–504.

(6) Yu, Z.; Wang, Z.; Daniel Adenutsi, C. Genesis of Authigenic Clay Minerals and Their Impacts on Reservoir Quality in Tight Conglomerate Reservoirs of the Triassic Baikouquan Formation in the Mahu Sag, Junggar Basin. *Western China. Mar. Pet. Geol.* **2023**, *148*, No. 106041.

(7) Chafeet, H. A.; Handhal, A. M. Evaluating the Zubair Reservoir (Main Pay) in Selected Wells of the Rumaila Oilfield, Southern Iraq, Using Nuclear Magnetic Resonance Logging and Petrophysical Analysis Data. *Carbonates and Evaporites* **2024**, *39* (3), 65.

(8) Lai, J.; Su, Y.; Xiao, L.; Zhao, F.; Bai, T.; Li, Y.; Li, H.; Huang, Y.; Wang, G.; Qin, Z. Application of Geophysical Well Logs in Solving Geologic Issues: Past, Present and Future Prospect. *Geosci. Front.* **2024**, *15*, No. 101779.

(9) Chafeet, H. A.; Handhal, A. M. Petrophysical, NMR, and MDT Analysis to Evaluate the Zubair Formation in the Rumaila Oilfield, Southern Iraq. *Arab. J. Geosci.* **2024**, *17* (4), 127.

(10) Harris, N. B.; Freeman, K. H.; Pancost, R. D.; Mitchell, G. D.; White, T. S.; Bate, R. H. *Patterns of Organic-Carbon Enrichment in a Lacustrine Source Rock in Relation to Paleo–Lake Level, Congo Basin, West Africa*. 2005.

(11) Behar, F.; Delhaye-Prat, V.; Garel, S. Detrital Input Quantification in Lacustrine Petroleum Systems: An Example of the Pre-Salt Source Rocks from the Lower Congo Basin (Congo). *Depos. Rec.* **2021**, *7* (1), 147–171.

(12) Bah, B.; Lacombe, O.; Beaudoin, N. E.; Zeboudj, A.; Gout, C.; Girard, J.-P.; Teboul, P.-A. Paleostress Evolution of the West Africa Passive Margin: New Insights from Calcite Twinning Paleopiezometry in the Deeply Buried Syn-Rift TOCA Formation (Lower Congo Basin). *Tectonophysics* **2023**, *863*, No. 229997.

(13) Cole, G. A.; Requejo, A. G.; Ormerod, D.; Yu, Z.; Clifford, A. *AAPG Memoir 73, Chapter 23: Petroleum Geochemical Assessment of the Lower Congo Basin*; AAPG 2000.

(14) Mutti, E. *Turbidite Sandstones*; AGIP, Istituto di geologia, Università di Parma, 1992.

(15) Manzoor, U.; Ehsan, M.; Hussain, M.; Iftikhar, M. K.; Abdelrahman, K.; Qadri, S. M. T.; Arshad, F.; Ashraf, K.; Fnais, M. S. Harnessing Advanced Machine-Learning Algorithms for Optimized Data Conditioning and Petrophysical Analysis of Heterogeneous, Thin Reservoirs. *Energy Fuels* **2023**, *37* (14), 10218–10234.

(16) Moon, M. S.; Pederson, J. M.; Osmon, K.; Al-Saied, M.; Al-Sabea, S. H.; Al-Shammari, H. Application of Petrophysically Derived" Flow Facies" for Reservoir Characterization and Simulation: Wara Reservoir, Greater Burgan Field. *SPE Annu. Technol. Conf. Exhib.*; SPE 1998, *49217*

(17) Elabsy, I.; AlTurkey, S.; Alhazzaa, S.; Dutta, A.; Belhouchet, M.; Abba, A. *Integration of Penta-Combo LWD Measurements for Petrophysical and Geomechanical Feasibility*; Abu Dhabi International Petroleum Exhibition & Conference, 2018.

(18) Movahhed, A.; Bidhendi, M. N.; Masihi, M.; Emamzadeh, A. Introducing a Method for Calculating Water Saturation in a Carbonate Gas Reservoir. *J. Nat. Gas Sci. Eng.* **2019**, *70*, No. 102942.

(19) Bello, A. M.; Butt, M. N.; Hussain, A.; Amao, A. O.; Olariu, C.; Koeshidayatullah, A. I.; Malik, M. H.; Al-Hashem, M.; Al-Ramadan, K. Impact of Depositional and Diagenetic Controls on Reservoir Quality of Syn-Rift Sedimentary Systems: An Example from Oligocene-Miocene Al Wajh Formation, Northwest Saudi Arabia. *Sediment. Geol.* **2023**, *446*, No. 106342.

(20) Xia, H.; Perez, E. H.; Dunn, T. L. The Impact of Grain-Coating Chlorite on the Effective Porosity of Sandstones. *Mar. Pet. Geol.* **2020**, *115* (10423), No. 104237.

(21) Ali Khoudja, S. A.; Chellat, S.; Hacini, M.; Semiani, A. Petrography and Authigenic Chlorite in the Siegenian Reservoir Rocks, Berkine Basin, Eastern Algerian Sahara. *Arab. J. Geosci.* **2020**, *13*, 1–16.

(22) Wang, G.; Chang, X.; Yin, W.; Li, Y.; Song, T. Impact of Diagenesis on Reservoir Quality and Heterogeneity of the Upper Triassic Chang 8 Tight Oil Sandstones in the Zhenjing Area, Ordos Basin, China. *Mar. Pet. Geol.* **2017**, *83*, 84–96.

(23) Tao, S.; Gao, L.; Pan, Z. Swelling of Clay Minerals and Its Effect on Coal Permeability and Gas Production: A Case Study of Southern Qinshui Basin, China. *Energy Sci. Eng.* **2019**, *7* (2), 515–528.

(24) Beaufort, D.; Rigault, C.; Billon, S.; Billault, V.; Inoue, A.; Inoue, S.; Patrier, P. Chlorite and Chloritization Processes through Mixed-Layer Mineral Series in Low-Temperature Geological Systems–a Review. *Clay Miner.* **2015**, *50* (4), 497–523.

(25) Hong, D.; Cao, J.; Wu, T.; Dang, S.; Hu, W.; Yao, S. Authigenic Clay Minerals and Calcite Dissolution Influence Reservoir Quality in Tight Sandstones: Insights from the Central Junggar Basin, NW China. *Energy Geosci.* **2020**, *1* (1–2), 8–19.

(26) Zhu, S.; Wang, X.; Qin, Y.; Jia, Y.; Zhu, X.; Zhang, J.; Hu, Y. Occurrence and Origin of Pore-Lining Chlorite and Its Effectiveness on Preserving Porosity in Sandstone of the Middle Yanchang Formation in the Southwest Ordos Basin. *Appl. Clay Sci.* **2017**, *148*, 25–38.

(27) Zhao, H.; Ning, Z.; Zhao, T.; Zhang, R.; Wang, Q. Effects of Mineralogy on Petrophysical Properties and Permeability Estimation of the Upper Triassic Yanchang Tight Oil Sandstones in Ordos Basin, Northern China. *Fuel* **2016**, *186*, 328–338.

https://doi.org/10.1021/acsomega.4c08491
ACS Omega 2025, 10, 10081–10106

(28) Wang, R.; Shi, W.; Xie, X.; Zhang, W.; Qin, S.; Liu, K.; Busbey, A. B. Clay Mineral Content, Type, and Their Effects on Pore Throat Structure and Reservoir Properties: Insight from the Permian Tight Sandstones in the Hangjinqi Area, North Ordos Basin, China. *Mar. Pet. Geol.* **2020**, *115*, No. 104281.
(29) Wan, Q.; Fan, A.-P.; Yang, R.-C.; Lenhardt, N. Diagenetic Mineralogy and Its Effect on the Reservoir Properties of the Sandstones of the Permian of S120 Block (Sulige Gas Field), Ordos Basin, NW China. *J. Palaeogeogr.* **2022**, *11* (3), 360−386.
(30) Weibel, R.; Nielsen, M. T.; Therkelsen, J.; Jakobsen, F. C.; Bjerager, M.; Mørk, F.; Mathiesen, A.; Hovikoski, J.; Pedersen, S. S.; Johannessen, P. N.; Dybkjær, K. Illite Distribution and Morphology Explaining Basinal Variations in Reservoir Properties of Upper Jurassic Sandstones, Danish North Sea. *Mar. Pet. Geol.* **2020**, *116*, No. 104290.
(31) Liu, C.; Zhong, J.; Wang, X.; Cao, M.; Wu, J.; Zhang, S.; Wu, X.; Sun, N.; Du, Y.; Liu, Y. Petrological Characteristics and the Impact of Mineral Content on Reservoir Quality in Coal-Bearing Strata of Linxing Area, Eastern Margin of Ordos Basin, China. *Energy Explor. Exploit.* **2018**, *36* (4), 872−894.
(32) Kumar, S.; Chandra, D.; Hazra, B.; Vishal, V.; Pathegama Gamage, R. Nanopore Characteristics of Barakar Formation Shales and Their Impact on the Gas Storage Potential of Korba and Raniganj Basins in India. *Energy Fuels* **2024**, *38* (5), 3833−3847.
(33) Hu, X.; Huang, S. Physical Properties of Reservoir Rocks. In Hu, X.; H, S.; J, F. H., Eds.; *Physics of Petroleum Reservoirs*. Springer Mineralogy. Springer: Berlin, Heidelberg, 2017.
(34) Ahmad, K. M.; Kristaly, F.; Turzo, Z.; Docs, R. Effects of Clay Mineral and Physico-Chemical Variables on Sandstone Rock Permeability. *J. Oil Gas Petrochem Sci.* **2018**, *1* (1), 18−26.
(35) Worden, R. H.; Griffiths, J.; Wooldridge, L. J.; Utley, J. E. P.; Lawan, A. Y.; Muhammed, D. D.; Simon, N.; Armitage, P. J. Chlorite in Sandstones. *Earth-Science Rev.* **2020**, *204*, No. 103105.
(36) Kra, K. L.; Qiu, L.; Yang, Y.; Yang, B.; Shola Ahmed, K.; Camara, M.; Kouame, E. M. Depositional and Diagenetic Control on Conglomerate Reservoirs: An Example from the Fourth Member of Shahejie Formation in the Lijin Sag, Bohai Bay Basin, East China. *J. Pet. Sci. Eng.* **2022**, *218*, No. 110913.
(37) Ma, Z.; Tan, J.; Zheng, L.; Ni, C.; Hu, R.; Ma, J. Simulation Experiment of Fluid-Feldspar Sandstone Interactions and Their Implications for Tight Oil and Gas Exploration of the Yanchang Formation, Ordos Basin, China. *Mar. Pet. Geol.* **2022**, *142*, No. 105737.
(38) Gao, J.; Ma, B.; Lu, Y.; Zhang, W.; Cao, Q. Origin of Authigenic Kaolinite with Implications for Permian Tight Gas Sandstone Reservoirs in the Northern Ordos Basin, Central China. *J. Nat. Gas Sci. Eng.* **2022**, *99*, No. 104429.
(39) Liu, K.; Wang, R.; Shi, W.; Travé, A.; Martín-Martín, J. D.; Baqués, V.; Qi, R.; Lin, J.; Ye, H. Diagenetic Controls on Reservoir Quality and Heterogeneity of the Triassic Chang 8 Tight Sandstones in the Binchang Area (Ordos Basin, China). *Mar. Pet. Geol.* **2022**, *146*, No. 105974.
(40) Zhao, D.; Hou, J.; Sarma, H.; Guo, W.; Liu, Y.; Xie, P.; Dou, L.; Chen, R.; Zhang, Z. Pore Throat Heterogeneity of Different Lithofacies and Diagenetic Effects in Gravelly Braided River Deposits: Implications for Understanding the Formation Process of High-Quality Reservoirs. *Geoenergy Sci. Eng.* **2023**, *221*, No. 111309.
(41) Yuan, G.; Cao, Y.; Schulz, H.-M.; Hao, F.; Gluyas, J.; Liu, K.; Yang, T.; Wang, Y.; Xi, K.; Li, F. A Review of Feldspar Alteration and Its Geological Significance in Sedimentary Basins: From Shallow Aquifers to Deep Hydrocarbon Reservoirs. *Earth-science Rev.* **2019**, *191*, 114−140.
(42) Vaisblat, N.; Harris, N. B.; Ayranci, K.; Chalaturnyk, R.; Power, M.; Twemlow, C.; Minion, N. Petrophysical Properties of a Siltstone Reservoir-An Example from the Montney Formation, Western Canada. *Mar. Pet. Geol.* **2022**, *136*, No. 105431.
(43) Nhunduru, R. A. E.; Jahanbakhsh, A.; Shahrokhi, O.; Wlodarczyk, K. L.; Garcia, S.; Maroto-Valer, M. M. The Impact of Wettability on Dynamic Fluid Connectivity and Flow Transport Kinetics in Porous Media. *Water Resour. Res.* **2022**, *58* (6), No. e2021WR030729.
(44) Kabir, P.; Akono, A. T. Fluid-Rock Reactions in Mt. Simon Sandstone at Microscopic Length-Scale. In *52nd US Rock Mechanics/Geomechanics Symposium*; OnePetro, 2018.
(45) Kimura, S.; Noda, S.; Minagawa, H. Experimental Investigation of Effects of Mica Content, Fe and Pressure on the Pore Size Distribution and Permeability of Sandy Sediment Using Proton Nuclear Magnetic Resonance. *Eng. Geol.* **2021**, *295*, No. 106408.
(46) Rasool, M. H.; Ahmad, M. Understanding Shale Instability through the Lens of Clay Mineralogy and Zeta Potential. *Geol. Earth Mar. Sci.* **2023**, *5* (2), 1.
(47) Baouche, R.; Ganguli, S. S.; Sen, S.; Radwan, A. E. Assessment of Reservoir Stress State and Its Implications for Paleozoic Tight Oil Reservoir Development in the Oued Mya Basin, Northeastern Algerian Sahara. *Geosystems and Geoenvironment* **2023**, *2* (1), No. 100112.
(48) Bahrami, N.; Dousi, N.; Lashari, A. Evaluation of Damage Mechanisms in Tight Gas Reservoirs: Integration of Laboratory Experiments and Field Data with Numerical Simulation. In *SPE offshore europe conference and exhibition*; SPE, 2015; p SPE-175433.
(49) Jia, K.; Zeng, J.; Wang, X.; Li, B.; Gao, X.; Wang, K. Wettability of Tight Sandstone Reservoir and Its Impacts on the Oil Migration and Accumulation: A Case Study of Shahejie Formation in Dongying Depression, Bohai Bay Basin. *Energies* **2022**, *15* (12), 4267.
(50) Herawati, I.; Permadi, P.; Rochliadi, A.; Marhaendrajana, T. Adsorption of Anionic Surfactant on Sandstone Reservoir Containing Clay Minerals and Its Effect on Wettability Alteration. *Energy Reports* **2022**, *8*, 11554−11568.
(51) Tiwari, B.; Ajmera, B. Consolidation and Swelling Behavior of Major Clay Minerals and Their Mixtures. *Appl. Clay Sci.* **2011**, *54* (3−4), 264−273.
(52) Zhao, X.; Yang, Z.; Lin, W.; Xiong, S.; Wei, Y. Characteristics of Microscopic Pore-Throat Structure of Tight Oil Reservoirs in Sichuan Basin Measured by Rate-Controlled Mercury Injection. *Open Phys.* **2018**, *16* (1), 675−684.
(53) Zhuang, Y.; Liu, X.; Xiong, H.; Liang, L. Microscopic Mechanism of Clay Minerals on Reservoir Damage during Steam Injection in Unconsolidated Sandstone. *Energy Fuels* **2018**, *32* (4), 4671−4681.
(54) Chen, Y.; Liu, D.; Fan, Q.; Zhang, C.; Li, Y.; Deng, Y.; Du, W.; Yin, W.; Zhang, Z.; Liu, L.; Luo, Q. Oil Mobility Evaluation of Fine-Grained Sedimentary Rocks with High Heterogeneity: A Case Study of the Lucaogou Formation in the Jimusar Sag, Junggar Basin, NW China. *Energy Fuels* **2023**, *37* (11), 7679−7695.
(55) Al-Yaseri, A.; Zhang, Y.; Ghasemiziarani, M.; Sarmadivaleh, M.; Lebedev, M.; Roshan, H.; Iglauer, S. Permeability Evolution in Sandstone Due to CO2 Injection. *Energy Fuels* **2017**, *31* (11), 12390−12398.
(56) Risha, M.; Douraghi, J. Impact of Clay Mineral Type on Sandstone Permeability Based on Field Investigations: Case Study on Labuan Island, Malaysia. In *Journal of Physics: Conference Series*; IOP Publishing, 2021; Vol. *1818*, p 12091.
(57) Abdel Azim, R.; Hamada, G. Novel Correlation for Calculating Water Saturation in Shaly Sandstone Reservoirs Using Artificial Intelligence: Case Study from Egyptian Oil Fields. *ACS omega* **2022**, *7* (34), 29666−29674.
(58) Vasconcelos, P. M.; Farley, K. A.; Malespin, C. A.; Mahaffy, P.; Ming, D.; McLennan, S. M.; Hurowitz, J. A.; Rice, M. S. Discordant K-Ar and Young Exposure Dates for the Windjana Sandstone, Kimberley, Gale Crater, Mars. *J. Geophys. Res. Planets* **2016**, *121* (10), 2176−2192.
(59) Golsanami, N.; Jayasuriya, M. N.; Yan, W.; Fernando, S. G.; Liu, X.; Cui, L.; Zhang, X.; Yasin, Q.; Dong, H.; Dong, X. Characterizing Clay Textures and Their Impact on the Reservoir Using Deep Learning and Lattice-Boltzmann Simulation Applied to SEM Images. *Energy* **2022**, *240*, No. 122599.
(60) Iranfar, S.; Karbala, M. M.; Shakiba, M.; Shahsavari, M. H. Effects of Type and Distribution of Clay Minerals on the Physico-

https://doi.org/10.1021/acsomega.4c08491
ACS Omega 2025, 10, 10081−10106

Chemical and Geomechanical Properties of Engineered Porous Rocks. *Sci. Rep.* **2023**, *13* (1), 5837.
(61) Lavaggi, T.; Muhammed, F.; Moretti, L.; Gillespie, J. W., Jr; Advani, S. G. Correlation of the Permeability and Porosity Development of Carbon/Carbon Composites during Pyrolysis. *Compos. Part A Appl. Sci. Manuf.* **2024**, *181*, No. 108156.
(62) Haj Messaoud, J.; Thibault, N.; Bomou, B.; Adatte, T.; Aljahdali, M. H.; Yaich, C. Integrated Surface-Subsurface Reservoir Zonation of the Early Bartonian Nummulitic Limestone in Central Tunisia and Eastern Tunisian Offshore. *Front. Earth Sci.* **2024**, *12*, No. 1452977.
(63) Starý, J.; Bruthans, J.; Schweigstillová, J.; Mareš, J.; Procházka, M. Origin of Fracture-Controlled Conduits in Calcite-Rich Highly Productive Aquifers Impregnated with Diagenetic Silica. *Water* **2024**, *16* (5), 687.
(64) Qu, Y.; Sun, W.; Wu, H.; Huang, S.; Li, T.; Ren, D.; Chen, B. Impacts of Pore-Throat Spaces on Movable Fluid: Implications for Understanding the Tight Oil Exploitation Process. *Mar. Pet. Geol.* **2022**, *137*, No. 105509.
(65) Zhang, L.; Xu, H.; Zhao, K.; Wang, J. Study on the Influencing Factors of Matrix Acidification Effect in Carbonate Reservoir. In *ARMA US Rock Mechanics/Geomechanics Symposium*; ARMA, 2024; p D022S024R004.
(66) Garing, C.; Gouze, P.; Kassab, M.; Riva, M.; Guadagnini, A. Anti-Correlated Porosity−Permeability Changes during the Dissolution of Carbonate Rocks: Experimental Evidences and Modeling. *Transp. Porous Media* **2015**, *107* (2), 595−621.
(67) Qajar, J.; Francois, N.; Arns, C. H. Microtomographic Characterization of Dissolution-Induced Local Porosity Changes Including Fines Migration in Carbonate Rock. *SPE J.* **2013**, *18* (03), 545−562.

https://doi.org/10.1021/acsomega.4c08491
ACS Omega 2025, 10, 10081−10106